SAND77-0601
Unlimited Release

A Tunable Diode Laser Heterodyne Spectrometer for Balloon-Borne Solar Radiometry in the Stratosphere

Colin E. Hackett

Prepared by Sandia Laboratories, Albuquerque New Mexico 87115
and Livermore, California 94550 for the United States Energy Research
and Development Administration under Contract AT (29-1) 789
Printed April 1977

Sandia Laboratories

SF 2900 Q(7-73)

DISCLAIMER

Issued by Sandia Laboratories, operated for the United States Energy Research & Development Administration by Sandia Corporation.

SAND 77-0601

Unlimited Release

A TUNABLE DIODE LASER HETERODYNE SPECTROMETER FOR BALLOON-BORNE SOLAR RADIOMETRY IN THE STRATOSPHERE*

Colin E. Hackett

Sandia Laboratories, Albuquerque, New Mexico 87115

ABSTRACT

A wavelength tunable infrared laser heterodyne spectrometer was taken into the stratosphere as part of the instrumentation package on board the stratospheric scientific research balloon, STRATCOM VI, in order to obtain high-resolution atmospheric absorption spectra of nitric oxide and water vapor by measurement of the attenuation of the solar radiance at approximately 5.24 microns. This report describes the development of this instrument system and the experimentation that characterized its performance.

Printed in the United States of America
Available from
National Technical Information Service
U.S. Department of Commerce
5285 Port Royal Road
Springfield, Virginia 22161
Price: Printed Copy $4.00; Microfiche $3.00

*This work was supported by the U.S. Energy Research and Development Administration with considerable assistance from the U.S. Army (Atmospheric Sciences Lab, White Sands, New Mexico), the U.S. Air Force (AF Cambridge Research Labs, Balloon Branch, and AFWL, Kirtland AFB, New Mexico), and the Massachusetts Institute of Technology, Lincoln Laboratory

ACKNOWLEDGEMENTS

I wish to thank Dr. Kumar Patel of Bell Laboratories for his help and encouragement in this endeavor. His efforts to promote laser spectroscopy and solar heterodyne radiometry in the stratosphere were crucial to this entire program.

Maj. Gilbert and his colleagues in the propagation section, Optics Branch, Air Force Weapons Laboratory, are thanked for their support, especially to the Solid State Research group of M.I.T. Lincoln Laboratory who supplied not only the tunable diode lasers and photovoltaic detectors but also much advice from Drs. Ivars Melngailis, Aram Mooradian, George Foyt, Robert Calawa and Dave Spears. The technical assistance from Herb Flicker, LASL, was also much appreciated.

Lastly, the enormous logistic support given in the other divisions in Sandia, especially by D. R. Smith, V. K. Smith, E. March, Al Woods (Sun Tracker), Rex Meyers, and Dave Werling is gratefully acknowledged.

TABLE OF CONTENTS

(THIS PAGE INTENTIONALLY LEFT BLANK.)

I. INTRODUCTION

The need to obtain accurate measurements of atmospheric nitric oxide (NO) concentrations in the unperturbed stratosphere has been recognized as being crucial to further understanding of the chemical and transport phenomena which govern the stability of the earth's ozone layer.[1,2] The wide ranges of results for nitric oxide concentration (2×10^7 to 2×10^9 molecules per cm^3) is sufficient to suggest that alternate techniques need to be developed to improve both the accuracy and the repeatability of this type of measurement.

The recent in situ measurements of nitric oxide made by Patel, et al[3] using a Raman spin-flip laser (carbon monoxide) spectrophone system gave values of nitric oxide concentration of about 2×10^9 molecules per cm^3 during high zenith sun conditions. This value is about a factor of ten larger than has been determined by Ridley, et al.[4] using a chemiluminescent in situ technique. The greatest discrepancy occurs during sunrise and sunset.

The Raman spin-flip laser spectrophone suffers from two important disadvantages for balloon borne measurements: its bulk and its weight cover 1000 kgm, which resulted in an altitude limit of about 30 km. The availability of advanced technology current injection wavelength tunable laser diodes from M.I.T. Lincoln Laboratory,[5] and the success of ground-based laser heterodyne measurements[6-8] prompted the development of a tunable laser heterodyne spectrometer system for balloon borne solar radiometry in the stratosphere. Such a system should have low weight, would be simple to operate remotely, and would have an inherent high spectral resolution capability (10 MHz, or about 3.3×10^{-4} cm^{-1}) to attempt Doppler limited spectroscopy, due to the absence of significant pressure broadening in the upper atmosphere.

II. LASER HETERODYNE RADIOMETER

The general arrangement of a laser heterodyne radiometer is shown in Fig. 1. Solar radiation is collected by a sun-tracking mirror and directed through a narrow

bandpass optical filter onto an infrared beam splitter. The radiation emanating from the tunable diode laser is collimated and directed to impinge on the beam splitter orthogonally to the optical axis of the filtered solar flux. A high-speed photovoltaic infrared detector is placed at the focus of a receiving lens which collects both diode laser radiation transmitted through the beam splitter, and solar radiation reflected from the beam splitter.

As a consequence of this arrangement, the photodetector will respond to the total effective electromagnetic energy field present at the receiver focus. The induced photocurrent in the photodetector will contain energy proportional to the product of the laser radiation electric field and the solar radiation electric field. If the photodetector is treated as a low impedance source similar to an antenna, it may be incorporated into a tuned circuit by inductively coupling it, through an intermediate frequency transformer, to a tuned amplifier. This electrical configuration limits the passage of heterodyne energy to that associated with the upper and lower sidebands of the electromagnetic spectrum:

$$\text{Upper side band: } (\nu_L + f^* - B/2) \text{ to } (\nu_L + f^* + B/2);\ \Delta f_u$$

$$\text{Lower side band: } (\nu_L - f^* - B/2) \text{ to } (\nu_L - f^* + B/2);\ \Delta f_L ,$$

where $\nu_L = 5.7 \times 10^{13}$ Hz, the nominal laser emission frequency (1906 cm^{-1}),

$f^* = 50$ MHz, the nominal intermediate frequency chosen, and

$B = 10$ MHz, the nominal bandwidth of the intermediate frequency circuits.

An estimate of the solar radiation at a nominal nitric oxide absorption wavelength of 5.24 μm can be obtained from Planck's spectral radiance function.

$$L(\lambda) = 2c^2h/[\lambda^5(e^{h\nu/kT}-1)] ,$$

where c = the speed of light, h = Planck's constant, ν = frequency, λ = wavelength, k = Boltzmann's constant, and T = solar temperature (5776 K). For $\lambda = 5.24$ μm,

$$L(\lambda) = 4.96 \times 10^4 \text{ watt } cm^{-2} \text{ -sr}^{-1} \text{ -cm}^{-1}.$$

The optical power received in the heterodyne passbands, Δf_u and Δf_L, of the photodetector is given by [9-12]

$$P_s(\lambda) = \frac{1}{2} L(\lambda) A_D \Omega \, S(\lambda) \, \Delta\lambda \quad ,$$

where A_D = detector's area, Ω = detector's field of view, $S(\lambda)$ = optical transmission of the atmosphere between the heterodyne receiver and the sun, and $\Delta\lambda$ = equivalent optical wavelength interval corresponding to the heterodyne passbands. From the antenna theorem,[10]

$$P_s(\lambda) = \frac{1}{2} L(\lambda) \, \lambda^2 \Psi \, S(\lambda) \, \Delta\lambda \quad ,$$

where Ψ is Yura's[9] correction factor for the finite size of the detector and the incoherent nature of the thermal source-radiation. For the geometries considered in this investigation, this factor is nearly equal to unity. The estimated optical power received in the heterodyne passbands due to the unattenuated solar flux ($S(\lambda) = 1$) is estimated to be about 1.25×10^{-12} watt.

The electrical power signal-to-noise ratio for a quantum noise limited photovoltaic detector is given by

$$(S/N)_{P,B} = \eta P_s(\lambda)/2h\nu B \quad ,$$

where η is the detector's quantum efficiency $= 0.5$ (for photovoltaic HgCdTe). Thus, the minimum detectable power, obtained by setting the signal-to-noise ratio to unity, is about 1.5×10^{-12} watt. Since this is only slightly more than the estimated power received by the detector passbands, some form of lock-in detection and amplification or signal correlation followed by integration must be employed to raise the effective signal-to-noise ratio to more acceptable values by reduction of the noise bandwidth. The voltage signal-to-noise ratio for a photovoltaic detector using a correlator with an effective integration time τ, may be expressed as

$$(S/N)_{V,C} = (S/N)_{P,B}^{\frac{1}{2}} = \eta \, \frac{(B\tau)^{\frac{1}{2}}}{2} \Big/ \left[e^{h\nu/kT} - 1 \right] \quad .$$

For τ = 0.1 sec, the effective value appropriate for nitric oxide measurement is a $(S/N)_{V,C}$ = 412 or about 52 db, which should be sufficient to carry out the solar heterodyne experiment. The requirements on the infrared detector, however, are extraordinary. It must have a high frequency response up to the intermediate frequency (f^* + 50 MHZ) and also a high quantum efficiency at the laser wavelength (5.24 μm). High-frequency response (up to 1.2 GHz) photovoltaic HgCdTe detectors, made available by M.I.T. Lincoln Laboratory,[5] are expected to provide satisfactory performance.

III. WAVELENGTH TUNABLE DIODE LASER LOCAL OSCILLATOR

The nominal emission frequency of the M.I.T. diode lasers is near 1906 cm^{-1}. For a typical tuning rate of about 10 cm^{-1} per ampere (injection current), these lasers are expected to pass through the R-branch absorption lines of nitric oxide corresponding to quantum numbers J = 15/2 to 21/2, i.e., from 1903.13 cm^{-1} and 1907.97 cm^{-1}. Two strong absorption lines of H_2O at 1907.96 cm^{-1} are also within this tuning range.

TABLE OF LINE FREQUENCIES OF DOMINANT ABSORBANTS

(WITHIN TUNING RANGE 1900-1912 cm^{-1})

Line Frequency cm^{-1}	Molecule	State/Transition
1900.07	NO	$R(13/2)_{\frac{1}{2}}$
1901.82	H_2O	$\nu_2(12_{3,10} - 11_{2,9})$
1903.13	NO	$R(15/2)_{\frac{1}{2}}$
1904.35	H_2O	$\nu_2(5_{3,3} - 4_{0,4})$
1906.14	NO	$R(17/2)_{\frac{1}{2}}$
1907.96	H_2O	$\nu_2(7_{4,4} - 6_{3,3})$
1909.13	NO	$R(19/2)_{\frac{1}{2}}$
1909.97	H_2O	$\nu_2(7_{3,4} - 6_{2,5})$
1912.08	NO	$R(21/2)_{\frac{1}{2}}$

Since the junction temperature of the diode laser should not exceed 15 K for optimum quantum efficiency, the laser is mounted on a cold finger attached at the bottom of a liquid helium dewar, as shown in Fig. 2. A concentric liquid nitrogen dewar provides thermal protection for the liquid helium dewar, and also provides a convenient mount for the HgCdTe heterodyne detector which must be maintained at 77 K in order to preserve its low noise and high quantum efficiency. To ensure minimum optical transmission losses, convex lenses are used as optical vacuum window elements to collimate radiation from the diode laser, and to focus the photomixed radiation on the detector. Problems of thermal shift of the optical axes due to temperature changes during the ascent are minimized by mounting turning mirrors and the IR beam splitter on a common box platform beneath the dewar.

IV. LASER OPERATION AND PERFORMANCE

Current-voltage curves for operating the M.I.T. tunable diode lasers indicate that conduction occurs for voltages above 200 mV; however, no significant laser action is observed for currents less than 0.6 amps. Once lasing has occurred, the current-voltage curve becomes nearly linear, with peak laser power occurring at about 1.5 amps. A typical current-voltage trace is shown in Fig. 3.

NO absorption spectra have been observed using a simple set up consisting of the diode laser source, absorption cell, and photovoltaic detector. Figure 4 shows the typical spectra that may be generated by ramping the injection current from about 0.6 to 2.4 amps. The upper trace was obtained with the intrinsic absorption in the laboratory air; the lower trace was obtained with the NO absorption cell (15 cm length and 67 Pascal pressure) in the optical path. Λ-type doubling is easily observed for the R-branch lines from the $^2\pi_{1/2}$ subband. Λ-type doubling for the same transitions from the $^2\pi_{3/2}$ subband is not as apparent since it is much smaller than in the $^2\pi_{1/2}$ subband, and is obscured by the intrinsic Doppler line width. Furthermore, the intensity of absorption is significantly larger for R branches of the $^2\pi_{1/2}$ subband, since the thermal occupation of the higher energy (123 cm^{-1}) $^2\pi_{3/2}$ multiplet is about 1/3 that of the $2\pi_{1/2}$ multiplet. For a comprehensive review of NO laser spectroscopy, refer to the work of Hinkley, Nill and Blum.[15]

Figure 5 shows a single scan of a Λ-type doublet for a current ramp from 1.1 to 1.2 amps; the upper trace is without the NO absorption cell in the optical path. Spectral stability of the diode laser was tested by the ability to overlay the output signal from the detector for 100 consecutive current ramps cycles. The result, shown in Fig. 6, indicates that the spectral stability should be sufficient for a signal processing technique using a correlator and integrator with a time constant of about 0.10 second.

V. PHOTOMIXING EXPERIMENTS

Several photomixing experiments have been carried out to determine the characteristics of the tuned electronic circuits that are coupled to the photovoltaic HgCdTe detector. These circuits responded in a satisfactory manner to the signal from a photomultiplier exposed simultaneously to radiation from a 632.8 nm HeNe laser and and from single side-band radiation from a 632.8 nm HeNe laser passing through a 40 MHz acousto-optic (Bragg) cell. Appropriate tuning of these circuits resulted in a nominal peak intermediate frequency of 52 MHz with a 3 db bandwidth of about 15 MHz. The spectral characteristic of the intermediate frequency amplifier is shown in Fig. 7.

The response of the video detector stage of the heterodyne circuit to a range of offset beam signal strengths is shown in Fig. 8. Ideally, the upper traces should closely approximate a square wave. The real device does exhibit some finite frequency response. The phenomenon of heterodyne detection is demonstrated by deliberately misaligning the Bragg offset beam. A comparison between the incoherent energy signal and the coherent energy signal is shown in Fig. 9. The layout for the visible wavelength photomixing experiments is illustrated in Fig. 10.

The response of the HgCdTe photovoltaic detector to an infrared heterodyne signal is also tested in a photomixing experiment shown in Fig. 11. Radiation from a 3.39 μm HeNe laser is passed through a beam splitter and one beam is directed onto a high speed spinning disk. The resulting Doppler shifted beam and the remaining unshifted beam are recombined optically on the HgCdTe detector. The resulting heterodyne signal, shown in Fig. 12, is observed on an oscilloscope.

VI. SUNTRACKING SYSTEM

The requirements for the suntracker and sun seeking mechanism are quite severe. Since the solar field of view from the earth is about 5 milliradians, a pointing accuracy of about 2.5 milliradians is required in order to keep at least half the solar disc incident on the optical axis of the radiometer during the data acquisition time.

The sun tracking mechanism used an elevation over azimuth mount. The azimuth axis including bearings, slip rings, and a direct drive DC servo motor was mounted centrally on the payload. The remainder of the tracking mechanism and the instrument were mounted on a table at the top of the azimuth shaft. The sensor for the tracking system was mounted on a horizontal shaft below the spectrometer. The sensor assembly contained both acquisition and tracking sensors and a target detector to sense the presence of the sun in the field of view of the tracking optics ($\approx 5°$). Silicon photo diodes were used as transducers in all of the sensing positions. The shaft which supported the sensor was driven directly by a D.C. servo motor. A mirror was mounted on a second shaft which was parallel to the sensor shaft. The two shafts were coupled by 2:1 low back lash gears. The mirror was adjusted to bisect the angle formed by the lines of sight of the tracking sensor and the spectrometer axis.

The severe accuracy requirements of the instrument made it necessary to use high gains in the tracking loops in order to maintain tracking accuracy. The scale factor of the type of tracking sensor used is highly sensitive to the intensity of the source which varies in this application with zenith angle of the sun. This made it necessary to use a conservative design in order to maintain suitable stability margins. These requirements made it necessary to use rate feedback in the tracking loops in order to maintain stability and accuracy. Rate gyros were mounted on the azimuth platform and the horizontal sensor axis to provide the required rate signals.

Figure 13 shows a block diagram of the tracking system. The acquisition sensors had a field of view of 180°. Control was switched to the tracking sensors when the sun was in the field of view of the target sensor as detected by the discriminator.

The loop gains in the acquisition mode were chosen to give sufficient accuracy so that the sun would enter the field of view of the tracking and target sensors. An additional control function (not shown in the diagram) was included to disable the tracking loops and command the mechanism to rotate at a constant rate in azimuth.

Since the balloon payload was known from previous flights to exhibit slow rotational motion about its vertical axis, the whole experiment was mounted on a platform which allowed continuous motion in either rotational direction. The electrical signals were transmitted from the main frame of the payload by low noise slip rings. Since the deployment of this experiment, a recent paper by Snider[14] points out the serious effects of refraction through the earth's atmosphere at infrared wavelengths. The effects of infrared refraction on the pointing accuracy were not fully appreciated and would require the use of infrared sunseeking optics rather than the visible optics employed in the current design.

VII. SIGNAL PROCESSOR SYSTEM

The operation of the signal processor system may be described in terms of the procedures required to extract the vertical optical absorption spectrum $S(\nu,h)$ at an optical frequency ν and atmospheric altitude h, from measurements of the angular heterodyne energy spectrum $e(\nu_L, \theta)$ obtain for a laser frequency ν_L and a solar zenith angle θ. The expression which relates $S(\nu,h)$ to $S(\nu,\theta)$ is

$$S(\nu,\theta) = \int_0^\infty \frac{S(\nu,h)dh}{\left[1 - \left(\frac{R}{R+h}\right)^2 \sin^2\theta\right]^{\frac{1}{2}}}$$

for a spherically symmetric atmosphere, where R is the earth's radius of curvature. As $h << R$ for balloon borne experimentation, then $S(\nu,h) = \frac{1}{h} S(\nu,\theta) \cdot \cos d$. Thus, the angular heterodyne energy spectrum $e(\nu_L,\theta)$ may be similarly transformed into an equivalent vertical energy spectrum, $e(\nu_L,h)$. The precise relationship between the heterodyne energy spectrum $e(\nu_L,h)$ and the atmospheric absorption spectrum $S(\nu,h)$ may be schematically described with reference to Fig. 14, which shows the

spectral relationship between the laser emission frequency ν_L, the associated upper and lower heterodyne passbands and the optical absorption spectrum. Since the solar emission spectrum which is received by the heterodyne detector is directly proportional to the absorption spectrum, the laser frequency ν_L may be swept across the absorption spectrum $S(\nu)$ to obtain the corresponding heterodyne energy spectrum $e(\nu_L)$ which will appear as shown in Fig. 14. In essence, $e(\nu_L)$ contains the superposition of both the upper side band absorption spectrum $S(\nu + f^*)$ and the lower side band absorption spectrum, $S(\nu - f^*)$. Should the absorption spectrum $S(\nu)$ contain features of spectral width Δf, then if $\Delta f < 2f^*$, these features will appear to be repeated by the process of passband superposition, otherwise there is a spectral spreading due to this effect. An approximate procedure for decomposition of this energy spectrum may be attempted by assuming that the form of the absorption spectrum close to a line center at ν_o is

$$S(\nu) = \frac{S(\nu_o)}{\pi} \frac{\Delta f}{[(\nu - \nu_o)^2 + \Delta f^2]} ,$$

where $S(\nu_o)$ is the line strength at ν_o, and Δf is the line width.

Thus, if the heterodyne energy spectrum $e(\nu) = c[S(\nu + f^*) + S(\nu - f^*)]$, where c is some arbitrary scaling coefficient, then

$$S(\nu) \simeq \frac{e(\nu)}{2c} \frac{1}{\left|1 + \sum_{n=1}^{\infty} \left(2f^*(\nu - \nu_o)\right)^{2n}\right|} .$$

As mentioned earlier, consideration of the expected signal-to-noise ratio indicates that some form of narrow band correlation and post-detection integration scheme should be used with the laser heterodyne radiometer. In the approach used here, the current ramp for the diode laser (operated at 656.25 Hz) is broken into 256 steps from the lower to the upper limits of the current range. Thus, the instantaneous laser emission frequency may be expressed as

$$\nu_L(t) = \frac{(\nu_2 - \nu_1)}{2\pi} \phi(t) ,$$

where ν_1 and ν_2 are the laser emission frequency limits and $\phi(t) = \omega t - 2k\pi$ is the time-dependent phase angle within the repetitive current ramp cycle, i.e., $\phi(t) = \sin^{-1}(\sin[\omega t])$, with k being some positive integer, and $\omega = 4{\cdot}123 \times 10^3$ r/s.

This is accomplished with the signal from a binary counter that is driven by a 168 kHz clock oscillator. The binary signal, when converted to an analog signal, is used to control the diode laser current by means of a conventional current regulated transistor circuit, see Fig. 15.

The response of the heterodyne radiometer to a given wavelength emitted by the diode laser is determined by correlating the output of the video detector stage with the corresponding current step in the ramp cycle. This is accomplished with a constant amplitude interrogating "position" pulse that is stepped sequentially across the ramp at a rate corresponding to 1% of the ramp frequency, see Fig. 16. This interrogating pulse is multiplied with the output from the video detector stage, and the product signal is integrated for a time corresponding to 100 ramp cycles for each step in the ramp current. The net effect of this "Box Car" integrator, is to average the heterodyne spectrum, in a step-wise fashion, over 2.5×10^4 ramp cycles.

Thus, the measured heterodyne energy phase spectrum, $e_D(\phi) = e(\phi) + e_N$, where e_N is the noise superposed on the ideal spectrum $e(\phi)$.

The "box car" averaged phase spectrum $\overline{e_c(\phi_i)}$ may be expressed as

$$\overline{e_c(\phi_i)} = \frac{1}{\tau} \int_t^{t+\tau} e(\phi[t]) + e_N)\ \delta(\phi_i, \Delta\phi)dt \quad ,$$

where $\delta(\phi_i, \Delta\phi)$ is a unity delta function representing the interrogating pulse of width $\Delta\phi$ and phase location ϕ_i; τ is the integration time = 100 t_r, see Fig. 17.

As $\Delta\phi = \frac{2\pi}{256}$, and $\phi_i = i{\cdot}\Delta\phi$, then the spectral resolution is $\Delta f = \frac{\nu_2 - \nu_1}{256}$.

Thus,

$$\overline{e_c(\phi_i)} \simeq \frac{1}{\tau} \int_t^{t+\tau} e(\phi[t]) \cdot \delta(\phi_i, \Delta\phi)dt \quad , \text{ if}$$

$$\int_t^{t+\tau} e_N \cdot \delta(\phi_2, \Delta\phi)dt \simeq 0$$

which is the case for an uncorrelated noise spectrum. A discrete form of the heterodyne energy spectrum may be constructed from this procedure, as shown in Fig. 18. A detailed description of the power supply and signal processing circuit is described by Meyers, et al.[13]

VIII. PRE-LAUNCH PREPARATIONS

In order to integrate the suntracker and seeker assemblies with the laser heterodyne spectrometer Dewar assembly, it was necessary to assure precise coincidence of the sun reflector mirror and the optical axis of the spectrometer. This was accomplished by determining the effective axis of the sun mirror and detecting the presence of an alignment laser beam both at 632.8 nm and 3.39 micron. The fact that the sunseeker system could not be tested with a far field source was a limitation to the pre-launch test procedure. A final check on the alignment of the sun mirror was accomplished with a retroreflecting mirror positioned on the detector side of the beam splitter, as shown in Fig. 1. Operation of the diode laser thus provided an alignment test, and also provided means of setting the upper and lower limits of the diode laser current injection ramp to assure correct location of the spectral interrogation of the laser heterodyne spectrometer. Figure 19 shows the results of tests that were performed to assure single mode operation of the laser diode. By placing a germanium etalon in the path of the laser beam and observing the transmission through the etalon, characteristic Fabray-Perot transmission peaks are observed. Should the laser be operating multimode, incomplete sinusoidal behavior would be seen in the etalon transmission data, thus indicating phase or frequency modulation. The other traces in Fig. 19 show the location of an NO absorption line, the intrinsic ground absorption, and the injection current ramp.

Figure 20 shows the configuration of the laser heterodyne spectrometer on the STRATCOM VI payload. The only optical interference expected is from the main support wires from the instrument frame to the balloon support line. This blockage is estimated to be about 2.6 milliradians per wire, and would obscure about half the solar disc should the wire remain directly in line with the solar azimuth throughout the correlator interation time. Since the balloon gondola is known to slowly rotate while stationary in altitude, the loss in sun seeking ability due to the four support wires is estimated

to be 1 part in 500. A closer view of the solar heterodyne radiometer assembly is shown in Fig. 21; the sun-seeking module may be seen on the left side below the infrared optical assembly.

The liquid helium transfer process is shown in Fig. 22. This procedure is accomplished about eight hours prior to launch. A final topping up of the cryogenic support is possible one hour before launch. At that time the cryogenic gas vent lines are attached. This procedure entails the fitting of a gauge pressure relief valve to establish a pressure of 1 atm above the cryogens at the 30 km float altitude. Figure 23 shows the radiometer assembly about one hour before launch.

IX. POST-LAUNCH OPERATION AND PERFORMANCE

The entire laser heterodyne radiometer system appeared to be operating satisfactorily for about 2 hours after launch. The first indication that trouble had occurred was a reading of an apparent zero liquid helium level at about 4 hours after launch. This was not discovered earlier since the normal assent procedure for balloon experimentation is to conserve power on ascent only by operating the monitoring systems intermittently.

At the time corresponding to sunrise, at the float altitude of the balloon, the instrumentation was turned on again. Unfortunately, the suntracker and sunseeker assembly had frozen during the ascent and did not become operational until about one hour after sunrise. This was very unfavorable since the critical composition measurements were of greatest significance during that period.

Upon reestablishing operation of the suntracker, it was possible to attempt operation of the laser heterodyne spectrometer, on the assumption that the liquid helium had not all boiled away. At this time a fault in the diode laser power supply was noticed. The power supply was unable to provide a complete ramp cycle. This feature was repeated each time the system was activated. Apparently, a wiring fault had developed after launch in the laser power supply which precluded proper operation. The Meyers and Werling[14] report on the power supply goes into this problem in greater detail.

The entire payload was recovered undamaged after some 35 hours aloft. The laser heterodyne radiometer was cycled through the usual pre-launch procedures and the Dewar filled with the appropriate cryogens. The diode laser exhibited a weakened diode characteristic, but was not burned out. Furthermore, the photodetector exhibited an almost perfect characteristic. These results are puzzling since if indeed the dewar had lost all its cryogens some 4 hours after launch and the heterodyne system had been operated for a total of some 50 minutes after that time, both the laser diode and the photodetector would have been damaged.

X. CONCLUSIONS

A self-contained wavelength-tunable laser heterodyne spectrometer was deployed to ascertain the atmospheric composition of nitric oxide and water vapor by measurement of the solar transmission spectra from a stratospheric balloon. The accomplishments may be summarized as follows:

1. System operations which appear to be satisfactory prior to launch:
   a. Wavelength tunable diode laser device and associated injection current power supply.
   b. Photovoltaic heterodyne detector and associated heterodyne energy measurement system.
   c. Photomixing optical system and associated sun-seeking system.
2. System operations which appear to be conditionally satisfactory prior to launch:
   a. Cryogens support system: This equipment did exhibit marginal performance prior to launch. Total cryogenic support time was measured at 19 hours when exposed to an external temperature of 210 K (-63°C).
   b. Sun tracking system: This system did exhibit marginal performance when tested at typical minimum temperatures.
3. System operations which did not appear to be satisfactory prior to launch:
   a. Inability to perform an actual solar heterodyne measurement on the

ground. This was due to the virtual elimination of solar radiation at 5.24 μm because of pressure-broadened water vapor in the lower atmosphere.

b. Inability to incorporate a self-calibration system into the spectrometer. This feature would have been included in the instrumentation had more preparation time been available prior to the launch date.

XI. RECOMMENDATIONS

It is recommended that the following problems should be solved before the diode laser heterodyne spectrometer can be considered a viable candidate for upper atmospheric composition measurements.

1. The spectral stability of the laser diode local oscillator should be determined by heterodyning a stabilized discretely tunable stabilized CO gas laser with the output of the tunable diode laser. It is important to determine the reproducibility of the output wavelength of the diode as functions of injection current and time.
2. Far-field quality of diode laser output.

   Tests should be carried out to determine if changes in the far-field output patterns of the diode laser will affect the heterodyne efficiency and whether astigmatic optics are needed.
3. Digital processing vs. analog processing.

   Tests should be carried out to determine the relative merits of digital processing vs. analog (lock-in or phase sensitive) processing of the heterodyne signals.

The utility of diode laser heterodyne spectroscopy for airborne applications will depend primarily on items (1) and (2). If the diode successfully passes these tests, the diode laser heterodyne spectrometer should be a viable candidate for airborne and remote applications requiring Doppler-limited spectral resolution.

XII. REFERENCES

1. Crutzen, P. J., "The Influence of Nitrogen Oxides on the Atmospheric Ozone Content," Quart. J. Roy. Meteorol. Soc. 96 , 320-325 (1970).

2. Johnston, H. S., "Reduction of Stratospheric Ozone by Nitrogen Oxide Catalysts from SST Exhaust," Science 173, 517-522 (1971).

3. Patel, C. K. N., Burkhardt, E. G. and Lambert, C.A.,"Spectroscopic Measurements of Stratospheric Nitric Oxide and Water Vapor," Science 184, 1173-1176 (1974).

4. Ridley, B. A., Schiff, H. I., Shaw, A., and Megill, L. R., "In Situ Measurements of Stratospheric Nitric Oxide Using a Balloon-Borne Chemiluminescent Instrument," J. Geophys. Res. 80, 1925-1929 (1975).

5. The diode lasers and photovoltaic detectors were made available by the Air Force Weapons Laboratory, Kirtland Air Force Base, Albuquerque, New Mexico 87117.

6. McElroy, J. H., "Infrared Heterodyne Solar Radiometery," Appl. Opt. 11, 1619-1622 (1972).

7. King, S. R., et al, "High-Resolution Atmospheric-Transmission Measurement Using a Laser Heterodyne Radiometer," Appl. Optics 12, 1106-1107 (1973).

8. Peyton, B. J., "An Infrared Heterodyne Radiometer for High-Resolution Measurements of Solar Radiation and Atmospheric Transmission," IEEE J. Quant. Elec. QE-11, 569-574 (1975).

9. Yura, H. T., "Optical Heterodyne Signal Power Obtained from Finite-Sized Sources of Radiation," Appl. Optics 13, 150 (1974).

10. Siegman, A. E., "The Antenna Properties of Optical Heterodyne Receivers," Proc. IEEE 54, 1350-1356 (1966).

11. Teich, M. C., "Infrared Heterodyne Detection," Proc. IEEE 56, 37-46 (1968).

12. Teich, M. C. and Yen, R. Y., "Three-Frequency Nonlinear Heterodyne Detection Parts 1 and 2," Appl. Optics 14, 666 (1975).

13. Myers, R. D., and Werling, D. K., "The Design of a Linear Ramp Current Supply for Balloon Borne Instruments," SAND 75-0659, Sandia Laboratories, Albuquerque, New Mexico 87115 (March 1976).

14. Snider, D. E., "Refractive Effects in Remote Sensing of the Atmosphere with Infrared Transmission Spectroscopy," J. Atmospheric Sci. 32, 2178-2184 (1975).

15. Hinkley, E. D., Nill, K. W., and Blum, F. A., "Infrared Spectroscopy with Tunable Lasers," in'Laser Spectroscopy of Atoms and Molecules,'Editor: Walther, E., Topics in App. Phys., Vol. 2, Springer-Verlag, Berlin-1976, pp. 127-197.

LIST OF FIGURE CAPTIONS

Figures	Captions
1	Schematic of laser heterodyne radiometer.
2	Engineering drawing of Janis Research Dewar used in laser heterodyne spectroscopy experiment.
3	Characteristic current-voltage curve for laser diode M.I.T. #3007.
4	Tunable laser spectroscopy of nitric oxide using M.I.T. laser #3007 and HgCdTe photovoltaic detector. Laser current injection from 0.60 to 2.40 amp in 1 ms. Upper Trace: Intrinsic absorption in lab. Lower Trace: Additional absorption with nitric oxide cell in place.
5	Tunable diode laser spectroscopy of nitric oxide using M.I.T. laser #3007 and HgCdTe photovoltaic detector. Laser current injection from 1.10 to 1.20 amp. Second trace shows single shot response and Λ-type doubling phenomenon.
6	Tunable diode laser spectroscopy using M.I.T. laser #3007 and HgCdTe photovoltaic detector. Narrow current range. Second trace shows 100 overlays to indicate laser's spectral stability.
7	Intermediate frequency amplifier spectral characteristic.
8	Radio-frequency spectral characteristic of intermediate frequency amplifier and detector stages of heterodyne circuit.
9	Oscillograph of spectral response of the heterodyne detection circuits to photocurrent from mixing HeNe laser and 40 MH_z Bragg cell single side band.
10	Schematic layout of HeNe (0.6328 μm) laser/ Bragg cell single side bank heterodyne experiment.
11	Schematic layout of HeNe (3.39 μm) laser Doppler heterodyne experiment.
12	Typical heterodyne signal from 3.39 μm laser Doppler heterodyne experiment.
13	Schematic diagram of the sun-tracker control system.
14	Relationship of the optical absorption spectrum $S(\nu)$ to the heterodyne energy spectrum $e(\nu_L)$.

List of Figure Captions (continued):

15	Schematics of the laser heterodyne radiometer logic and processor system.
16	Relationship between interrogating pulse and diode laser injection current ramp.
17	Development of final averaged heterodyne sign signal.
18	Discrete form of heterodyne spectrum.
19	Single mode operation verification test.
20	Photograph showing entire scientific instrumentation payload for STRATCOM VI balloon flight.
21	Photograph of solar heterodyne radiometer, sun tracker and rotational platform integrated into STRATCOM VI payload.
22	Liquid helium transfer operation for solar heterodyne radiometer in place on STRATCOM VI payload.
23	Solar heterodyne radiometer configuration one hour before balloon launch.

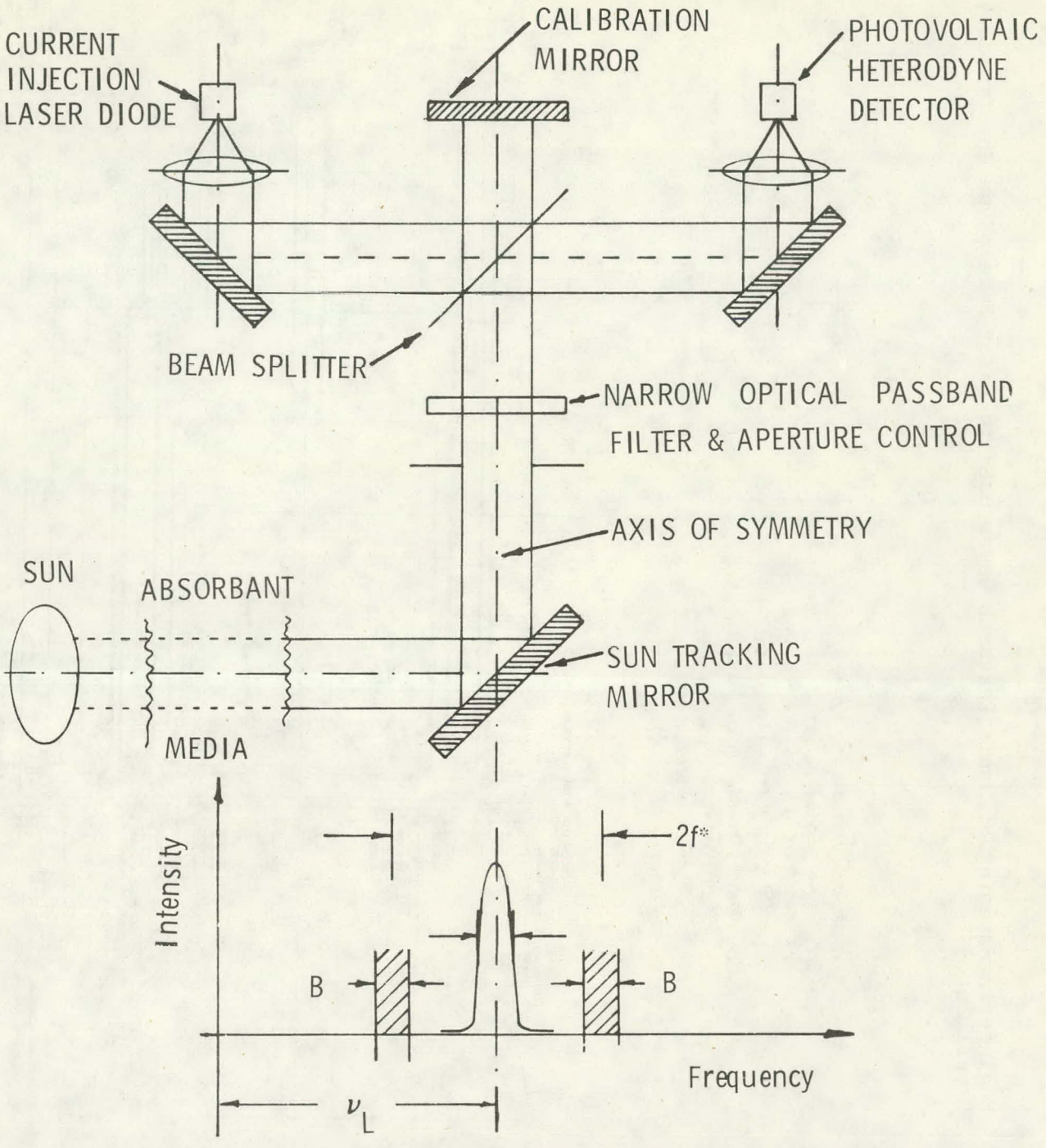

FIG. 1 SCHEMATIC OF LASER HETERODYNE RADIOMETER

Fig. 2 Engineering drawing of Janis Research Dewar used in Laser Heterodyne Spectroscopy Experiment.

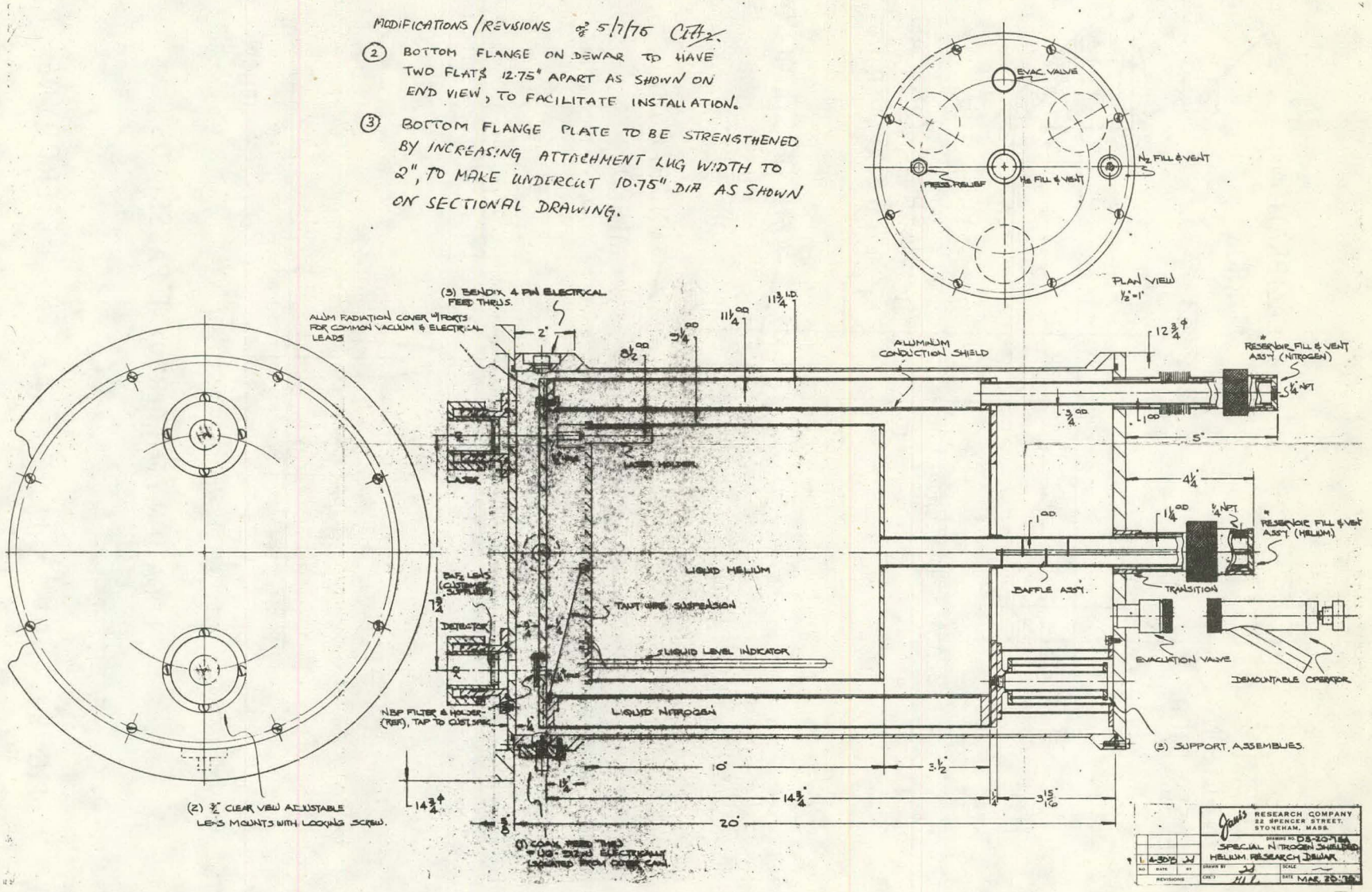

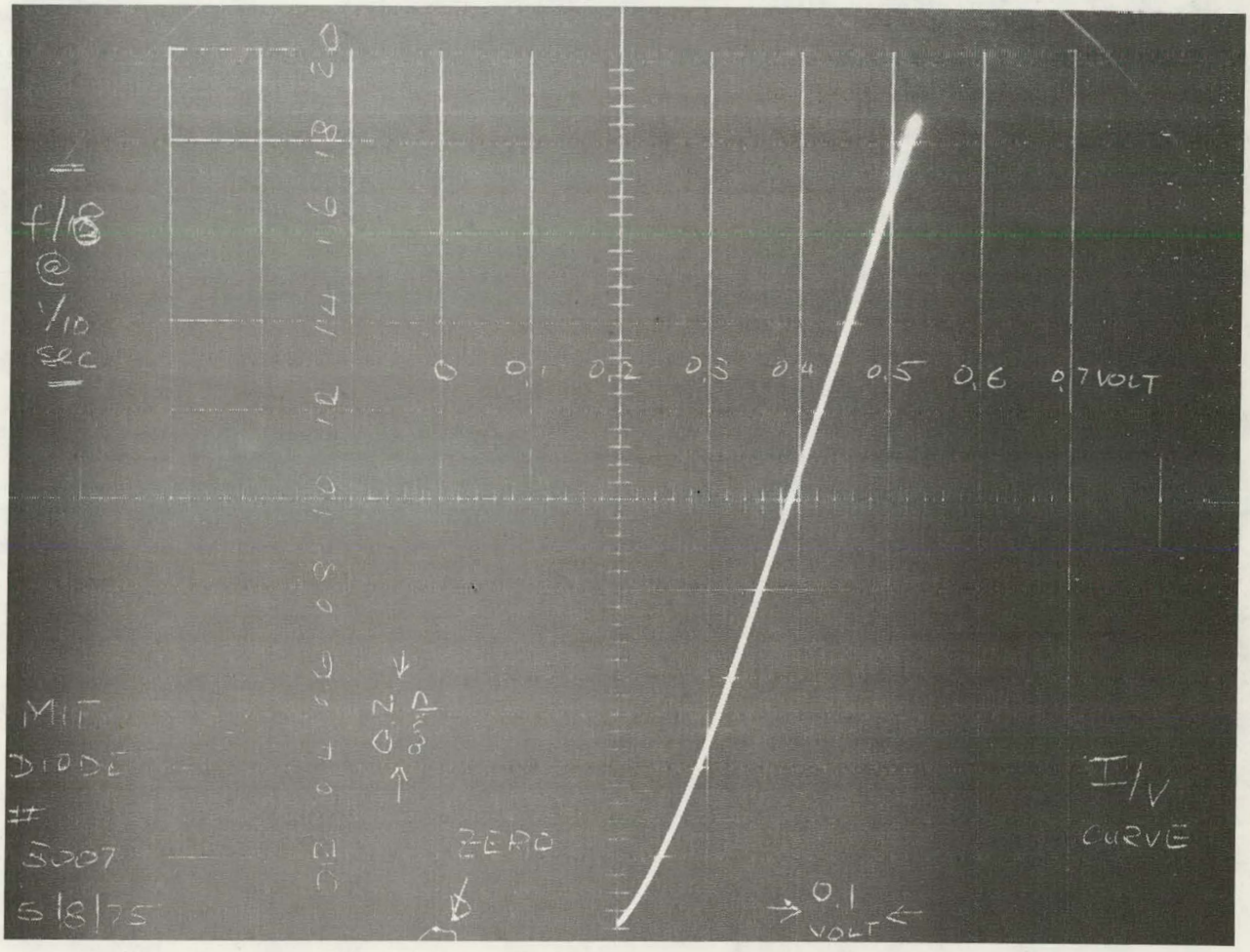

FIG. 3 CHARACTERISTIC CURRENT-VOLTAGE CURVE FOR LASER DIODE MIT # 3007

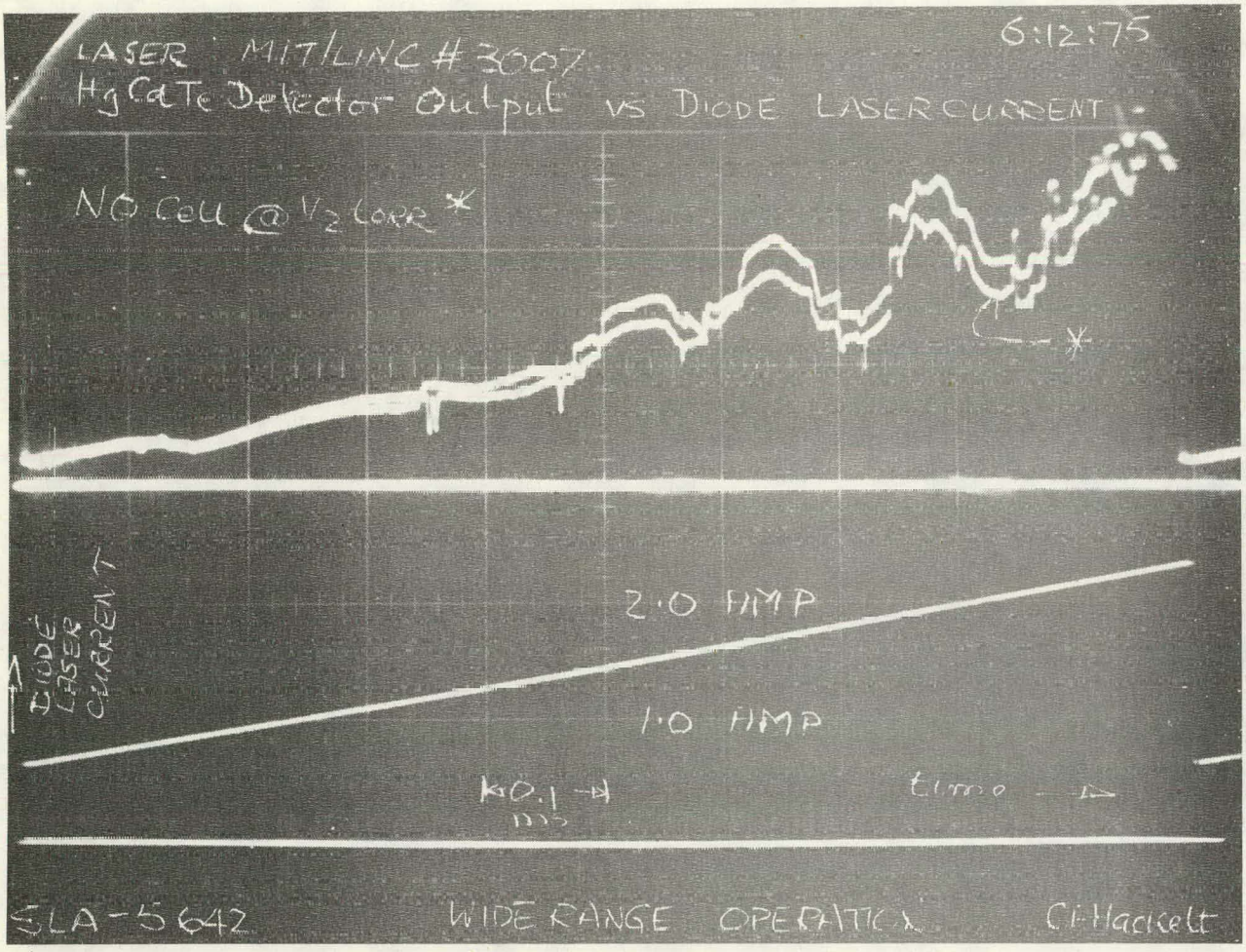

FIG. 4 TUNABLE DIODE LASER SPECTROSCOPY OF NICRIC OXIDE USING MIT LASER # 3007, AND HgCdTe PHOTOVOLTAIC DETECTOR. LASER CURRENT INJECTION FROM 0.60 to 2.40 AMP. IN 1 ms. UPPER TRACE: INTRINSIC ABSORPTION IN LABORATORY LOWER TRACE: ADDITIONAL ABSORPTION WITH NITRIC OXIDE CELL IN PLACE

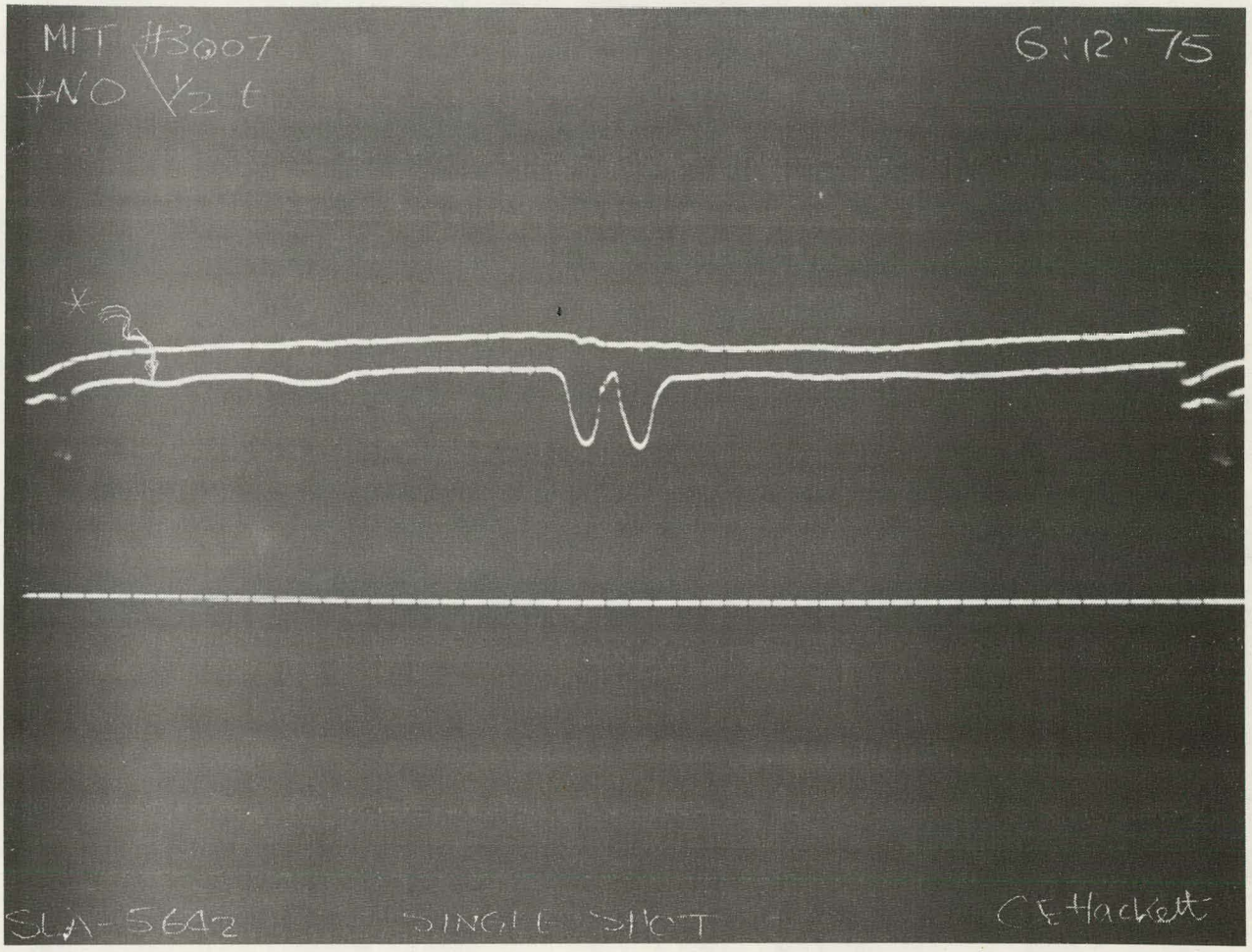

FIG. 5 TUNABLE DIODE LASER SPECTROSCOPY OF NITRIC OXIDE USING MIT LASER # 3007 AND HgCdTe PHOTOVOLTAIC DETECTOR. LASER CURRENT INJECTION FROM 1.10 to 1.20 AMP. SECOND TRACE SHOWS SINGLE SHOT RESPONSE, AND Λ TYPE DOUBLING PHENOMENON.

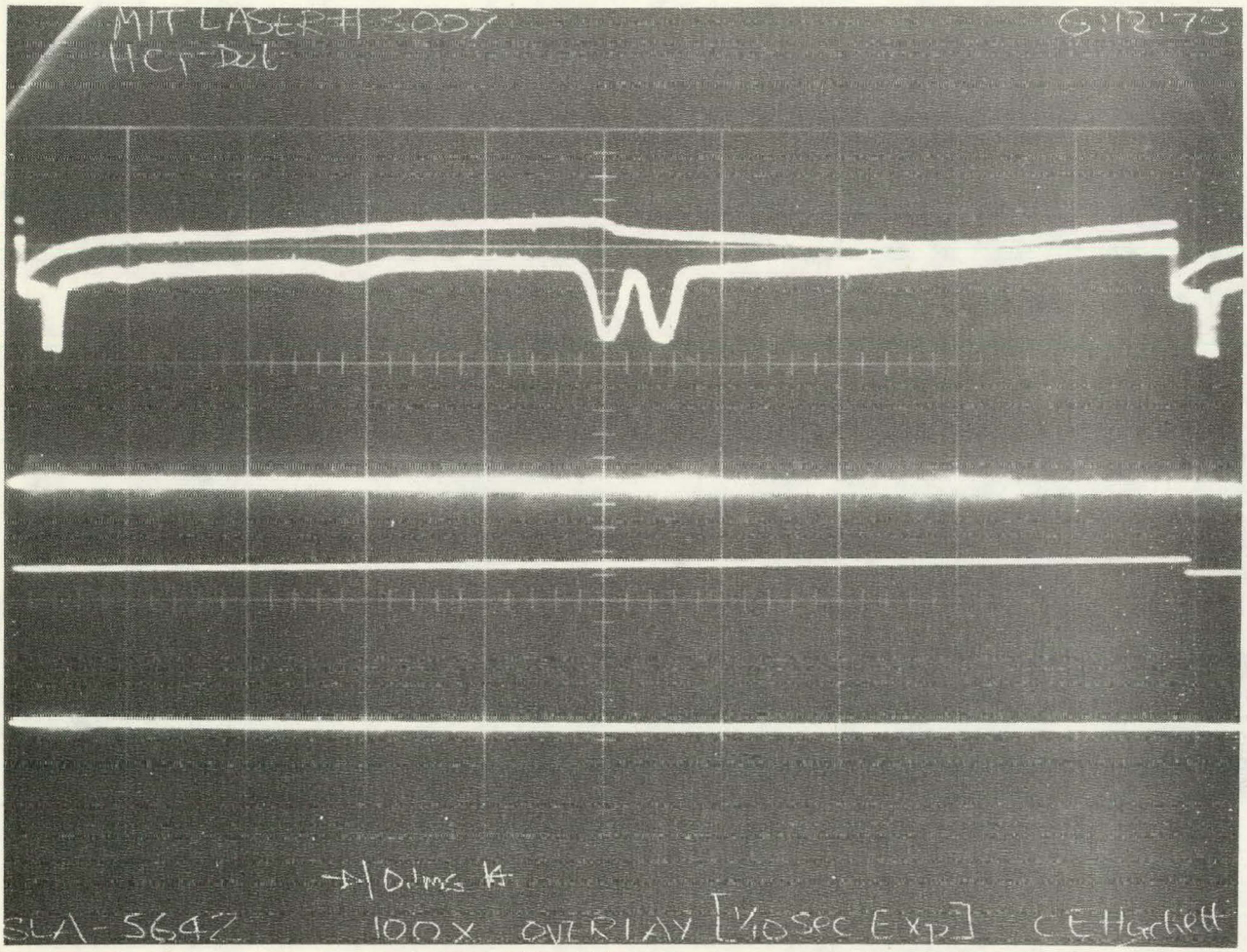

FIG. 6 TUNABLE DIODE LASER SPECTROSCOPY USING MIT LASER #3007 AND HgCdTe PHOTOVOLTAIC DETECTOR.
NARROW CURRENT RANGE.
SECOND TRACE SHOWS 100 OVERLAYS TO INDICATE LASER'S SPECTRAL STABILITY.

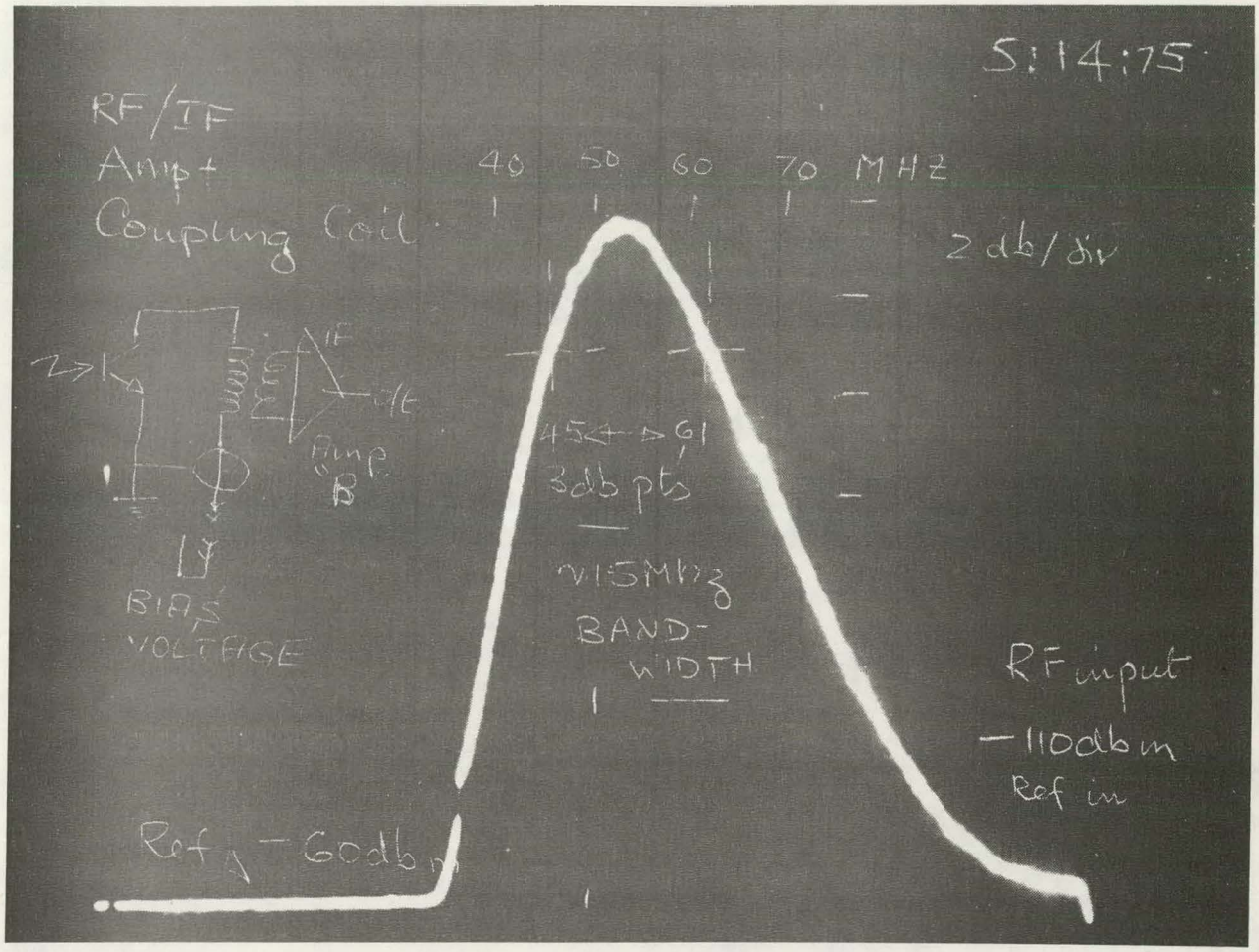

FIG. 7 INTERMEDIATE FREQUENCY AMPLIFIER SPECTRAL CHARACTERISTIC.

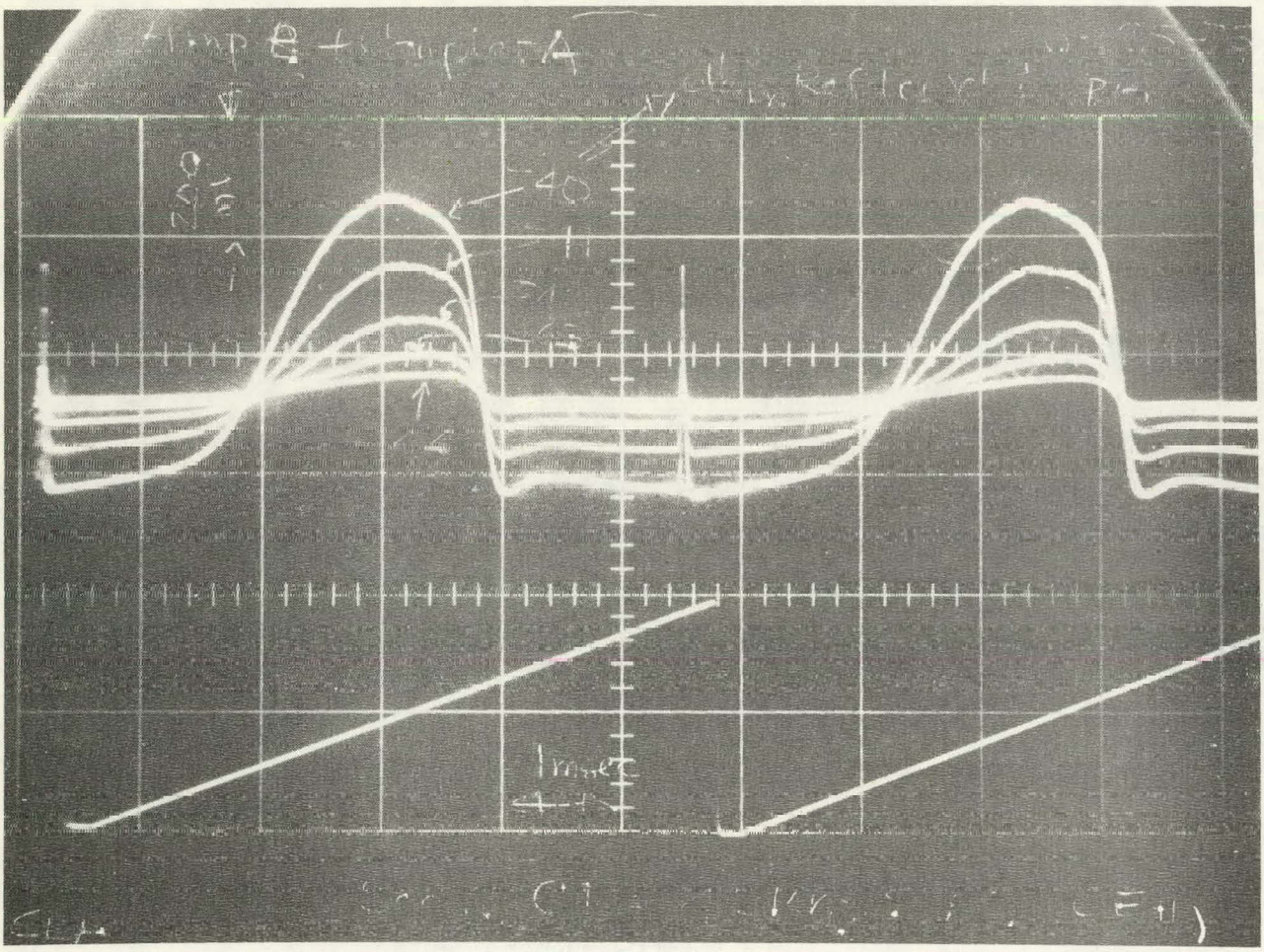

FIG. 8 RADIO FREQUENCY SPECTRAL CHARACTERISTIC OF INTERMEDIATE FREQUENCY AMPLIFIER AND DETECTOR STAGES OF HETERODYNE CIRCUIT.

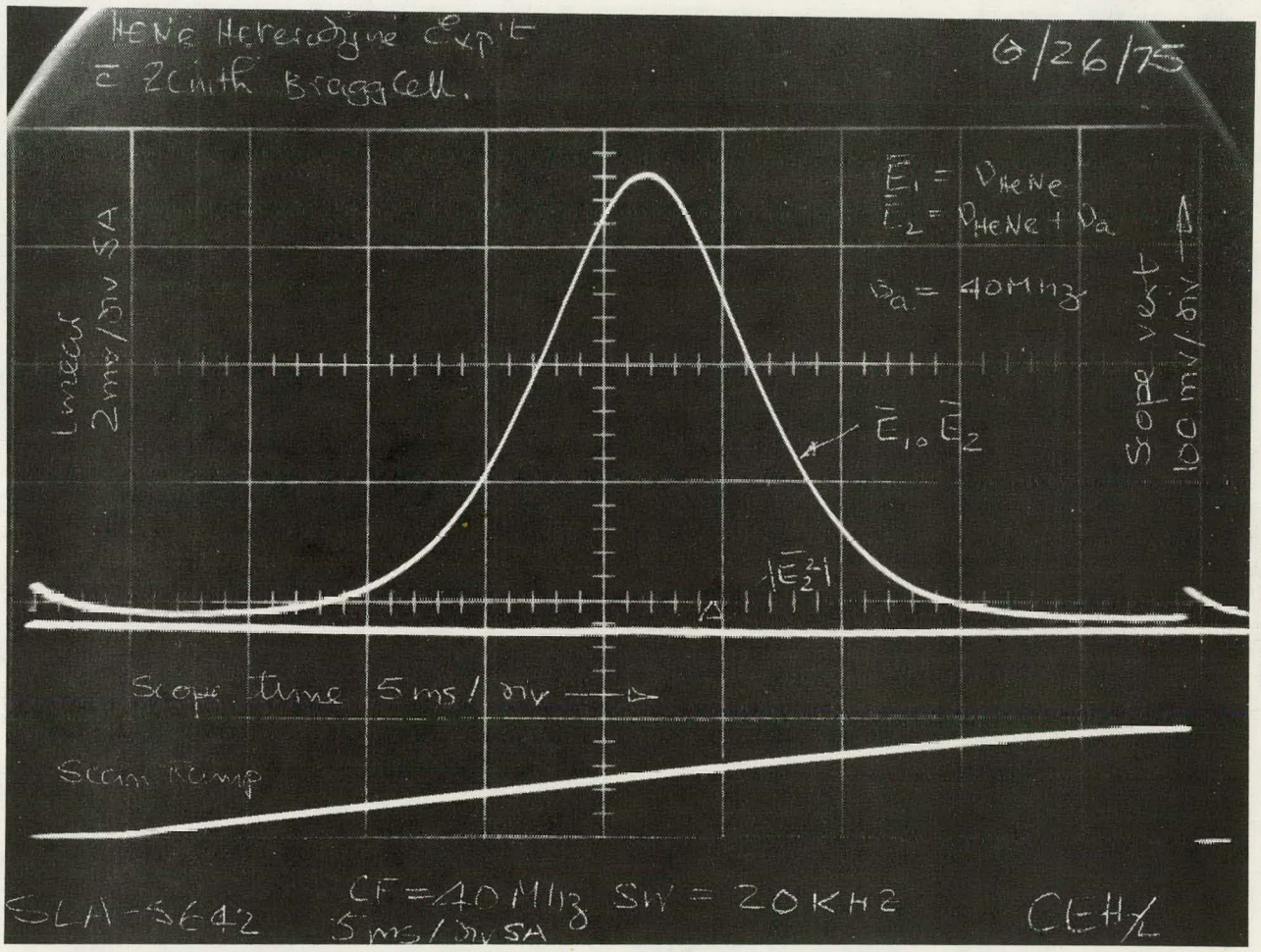

FIG. 9 OSCILLOGRAPH OF SPECTRAL RESPONSE OF THE HETERODYNE DETECTION CIRCUITS TO PHOTOCURRENT FROM MIXING HeNe LASER AND 40 MHz BRAGG CELL SINGLE SIDE BAND.

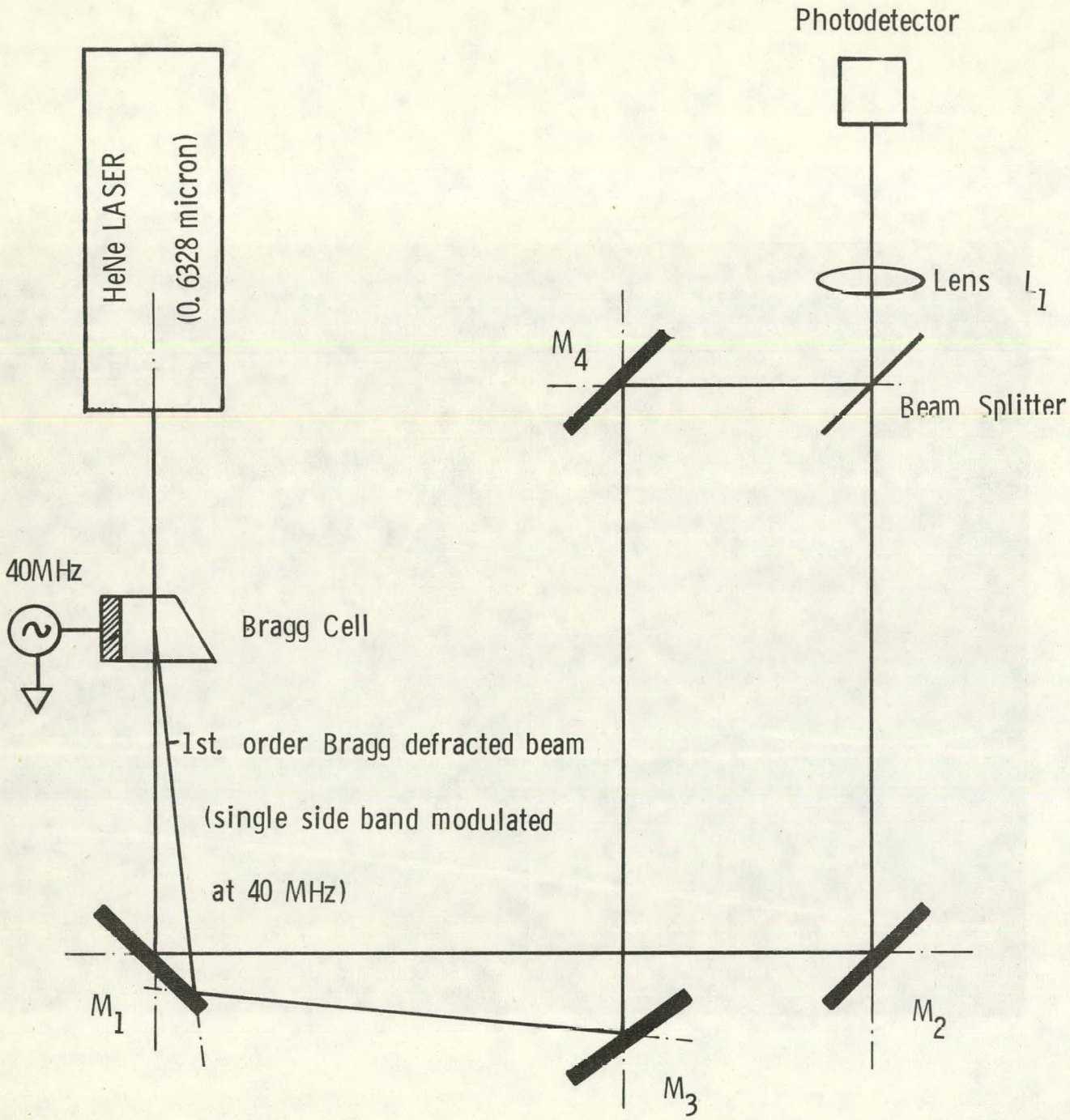

FIG. 10 SCHEMATIC LAYOUT OF HeNe (0. 6328 micron) LASER/ BRAGG CELL SINGLE SIDE BAND HETERODYNE EXPERIMENT.

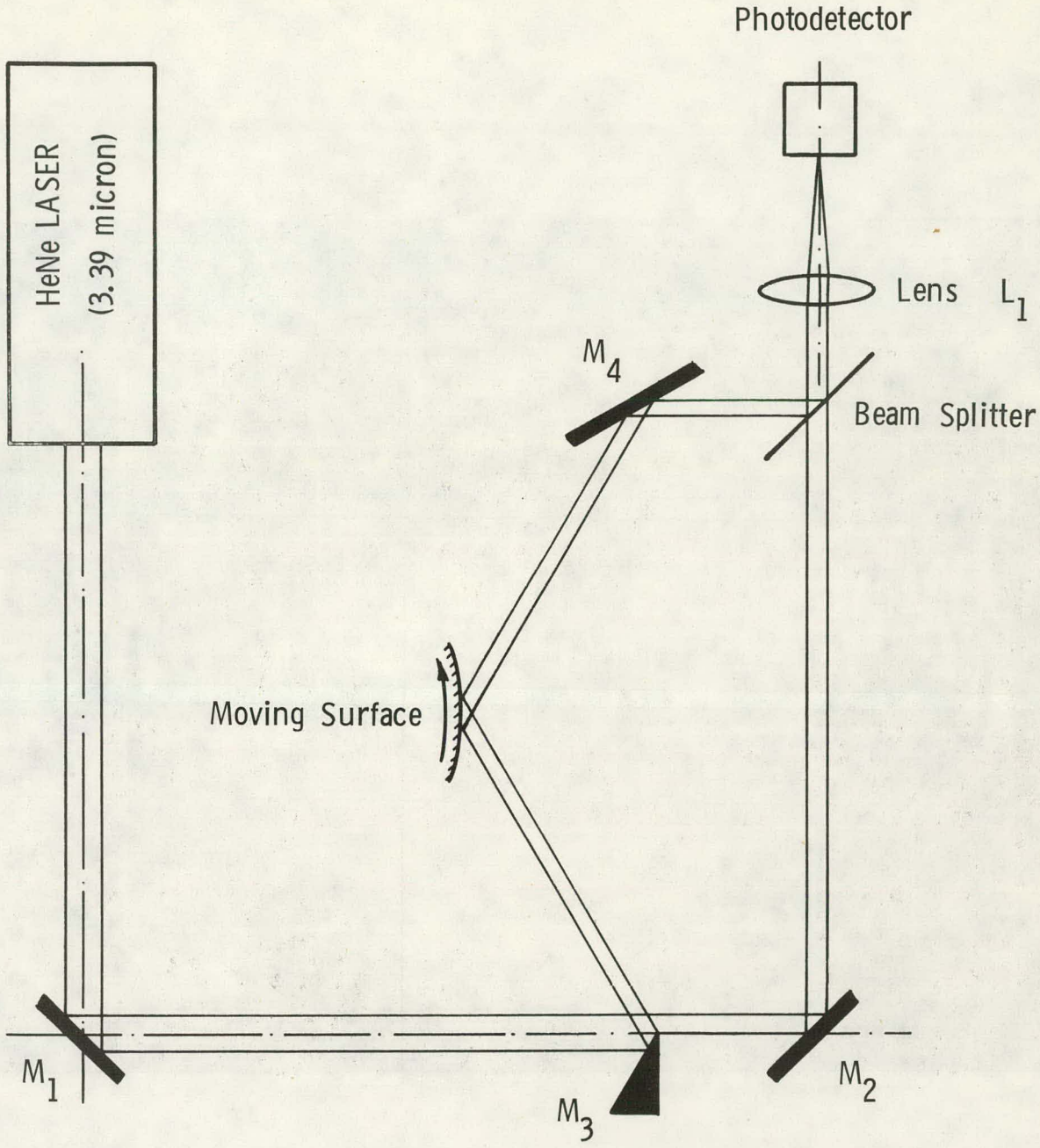

FIG. 11 SCHEMATIC LAYOUT OF HeNe (3.39 micron) LASER DOPPLER HETERODYNE EXPERIMENT.

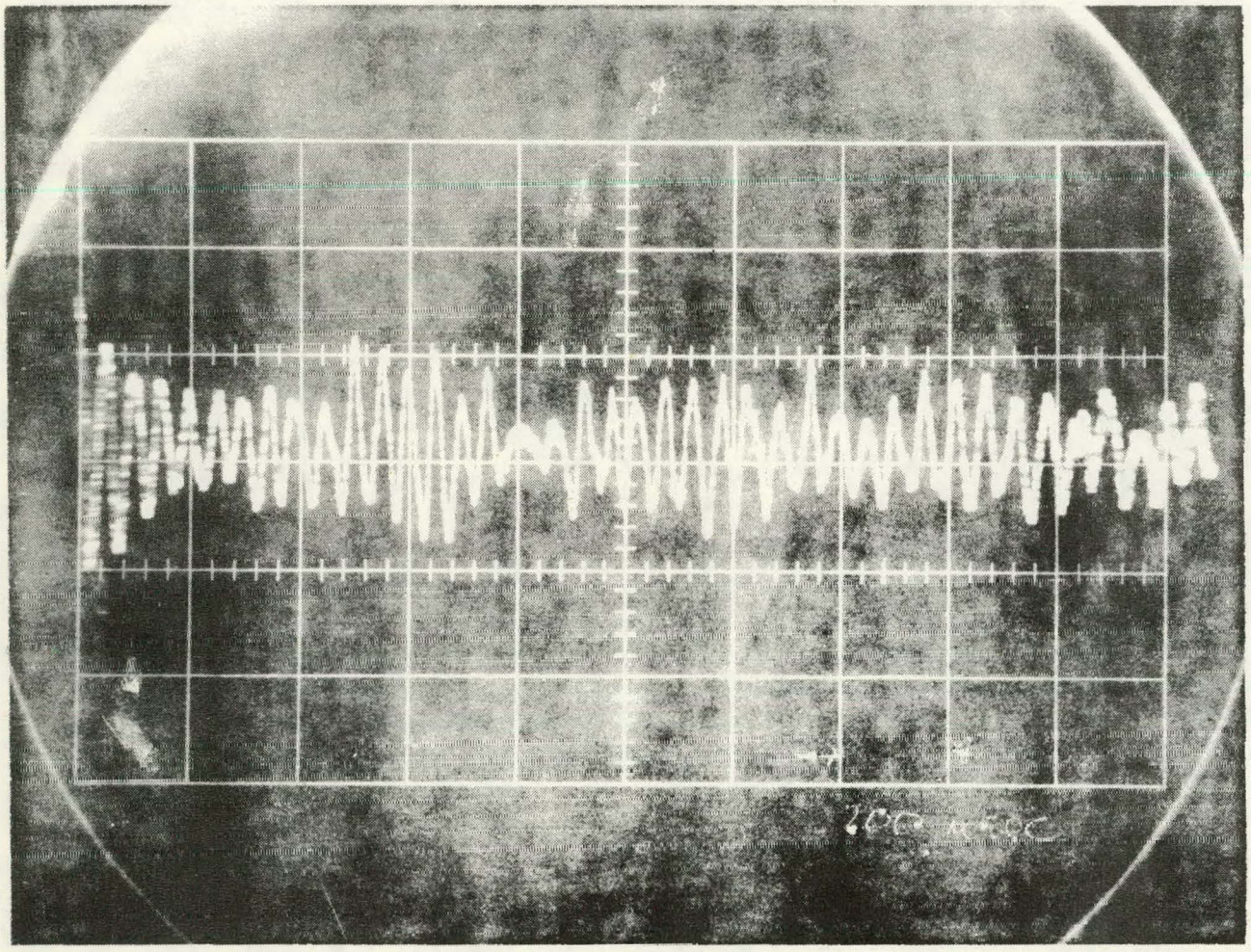

FIG. 12 TYPICAL HETERODYNE SIGNAL FROM 3.39 micron LASER DOPPLER HETERODYNE EXPERIMENT.

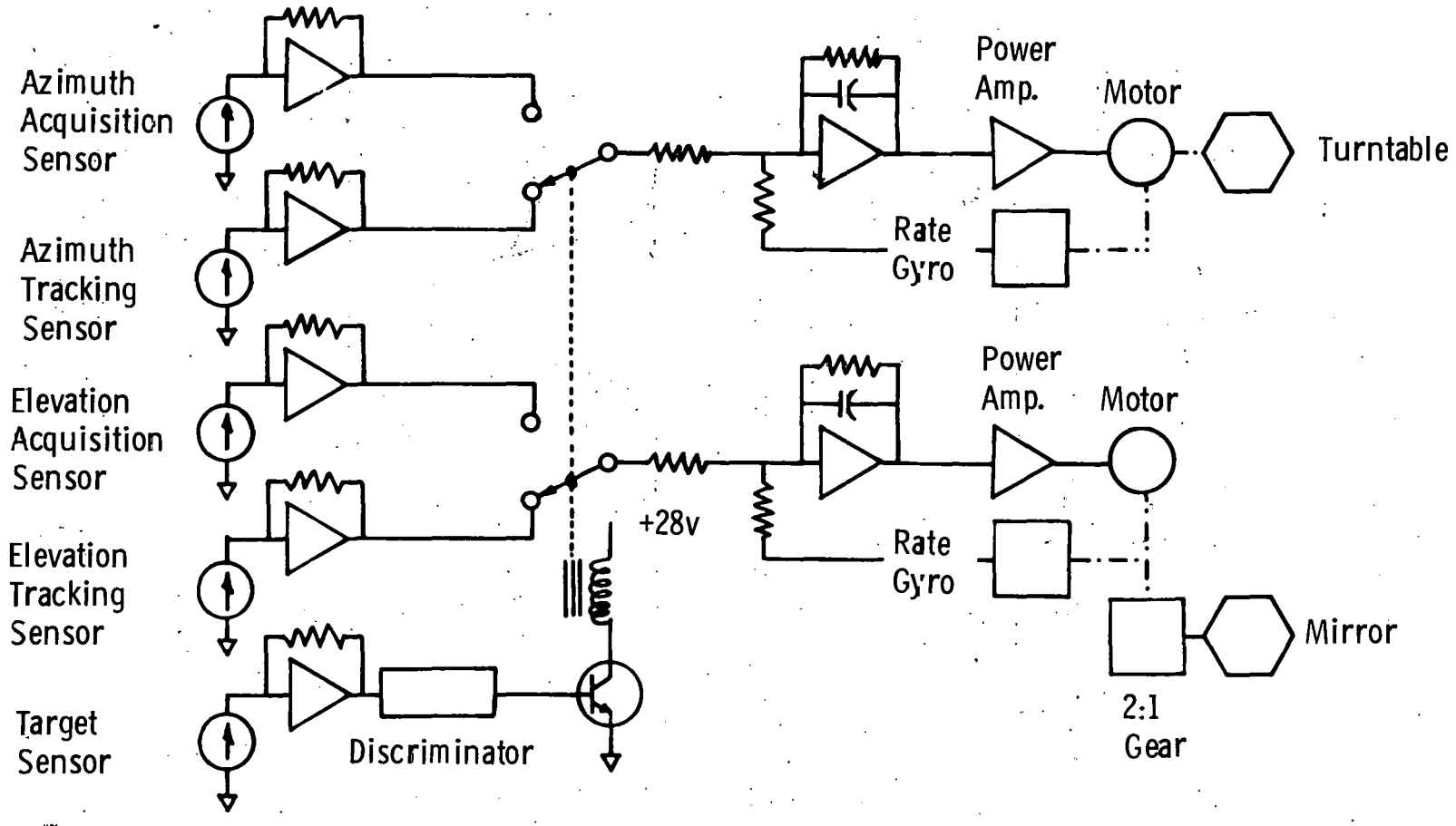

FIG. 13 SCHEMATIC DIAGRAM OF THE SUN-TRACKER CONTROL SYSTEM

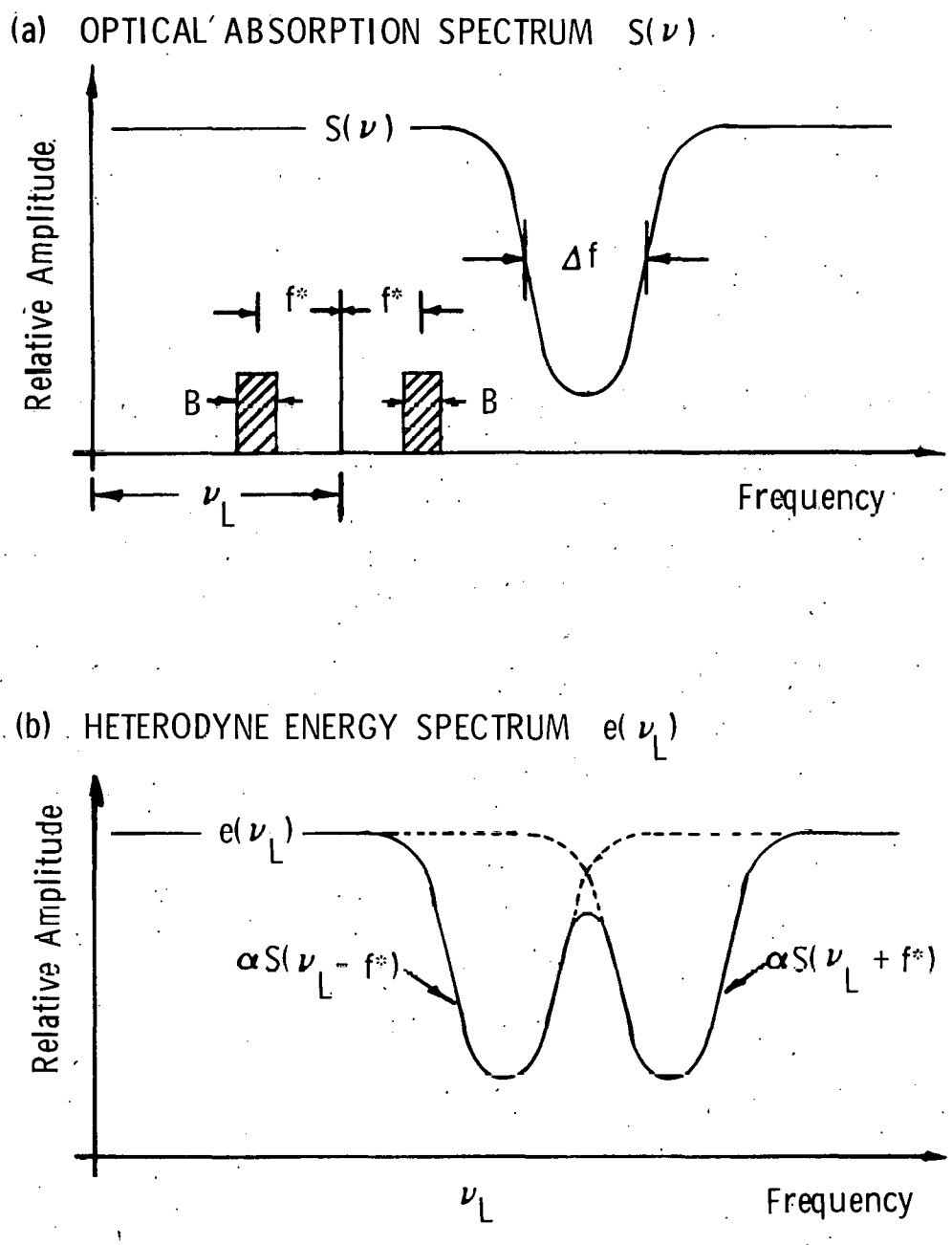

FIG. 14 RELATIONSHIP OF THE OPTICAL ABSORPTION SPECTRUM $S(\nu)$ TO THE HETERODYNE ENERGY SPECTRUM $e(\nu_L)$.

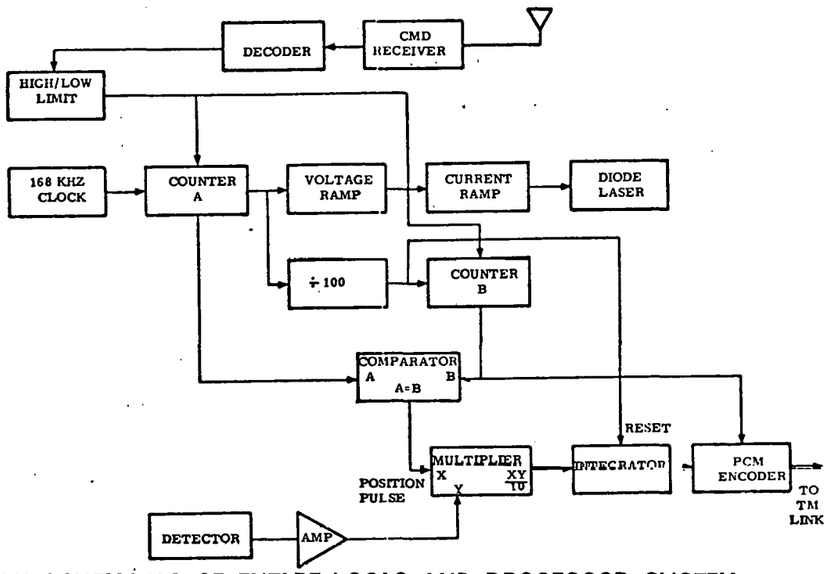

BLOCK SCHEMATIC OF ENTIRE LOGIC AND PROCESSOR SYSTEM

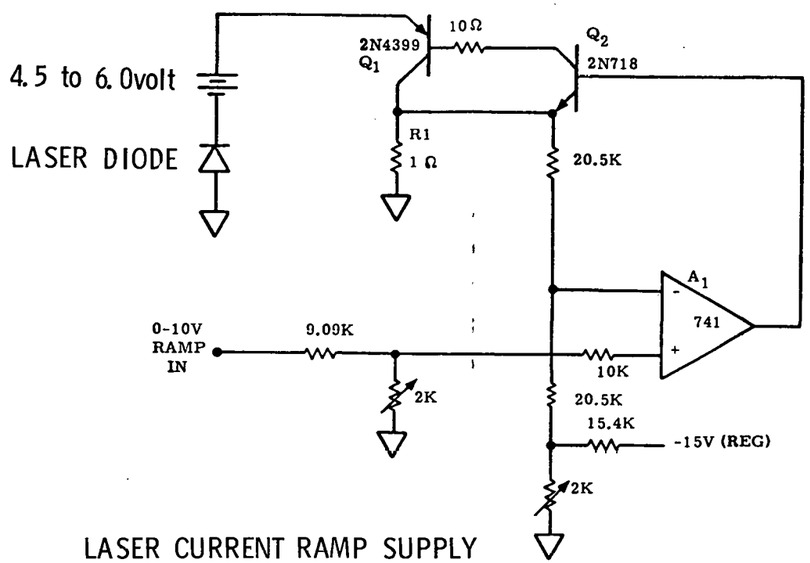

LASER CURRENT RAMP SUPPLY

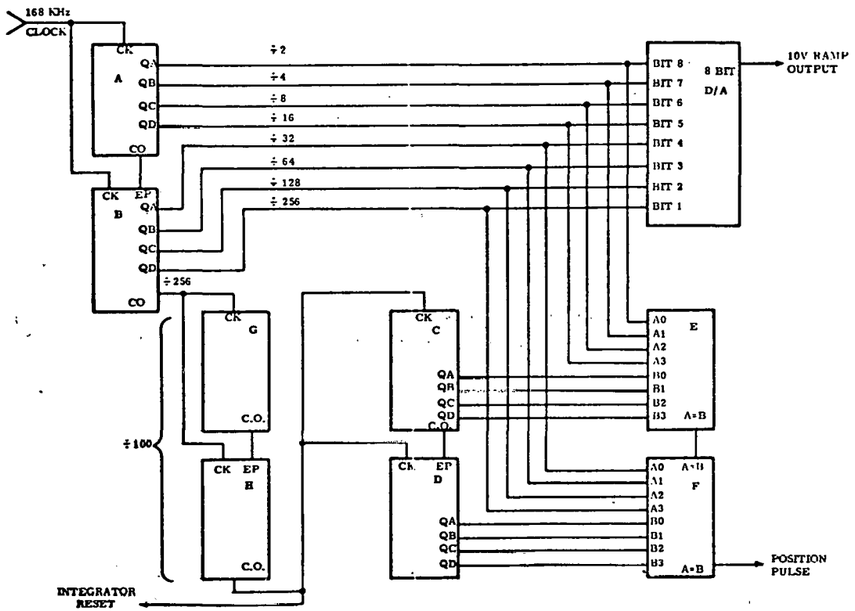

CIRCUIT USED TO GENERATE RAMP SIGNAL AND INTERROGATING PULSE

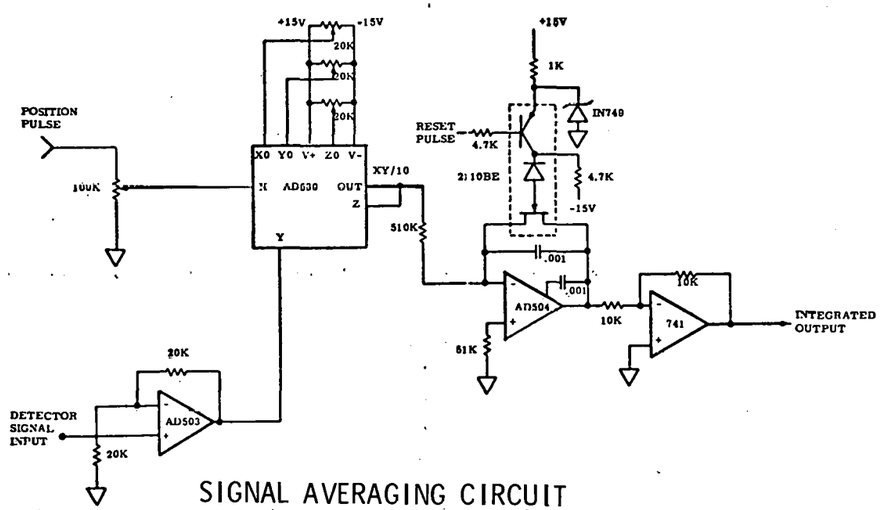

SIGNAL AVERAGING CIRCUIT

FIG. 15 SCHEMATICS OF THE LASER HETERODYNE RADIOMETER LOGIC AND PROCESSOR SYSTEM.

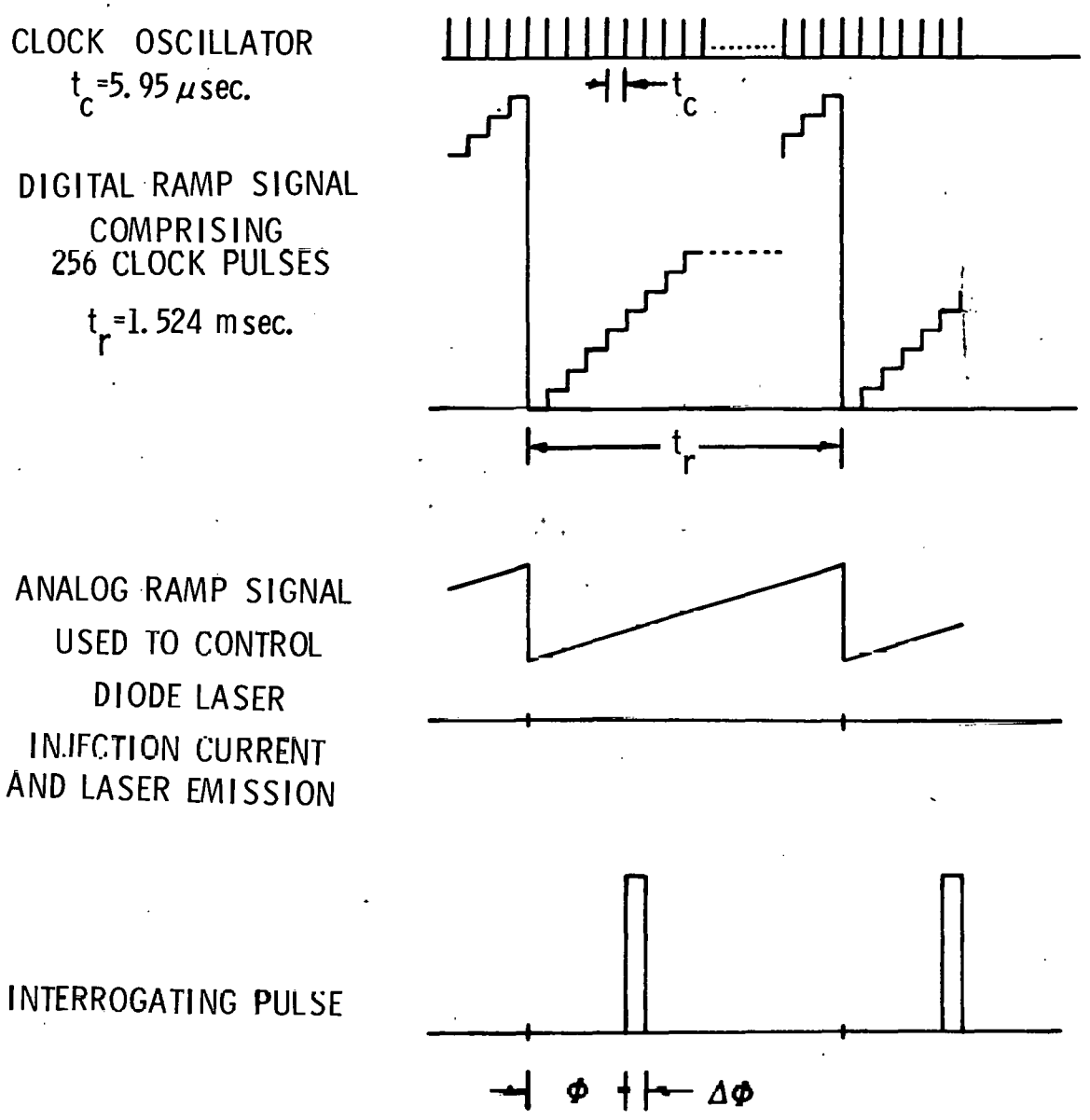

FIG. 16 RELATIONSHIP BETWEEN INTERROGATING PULSE AND DIODE LASER INJECTION CURRENT RAMP

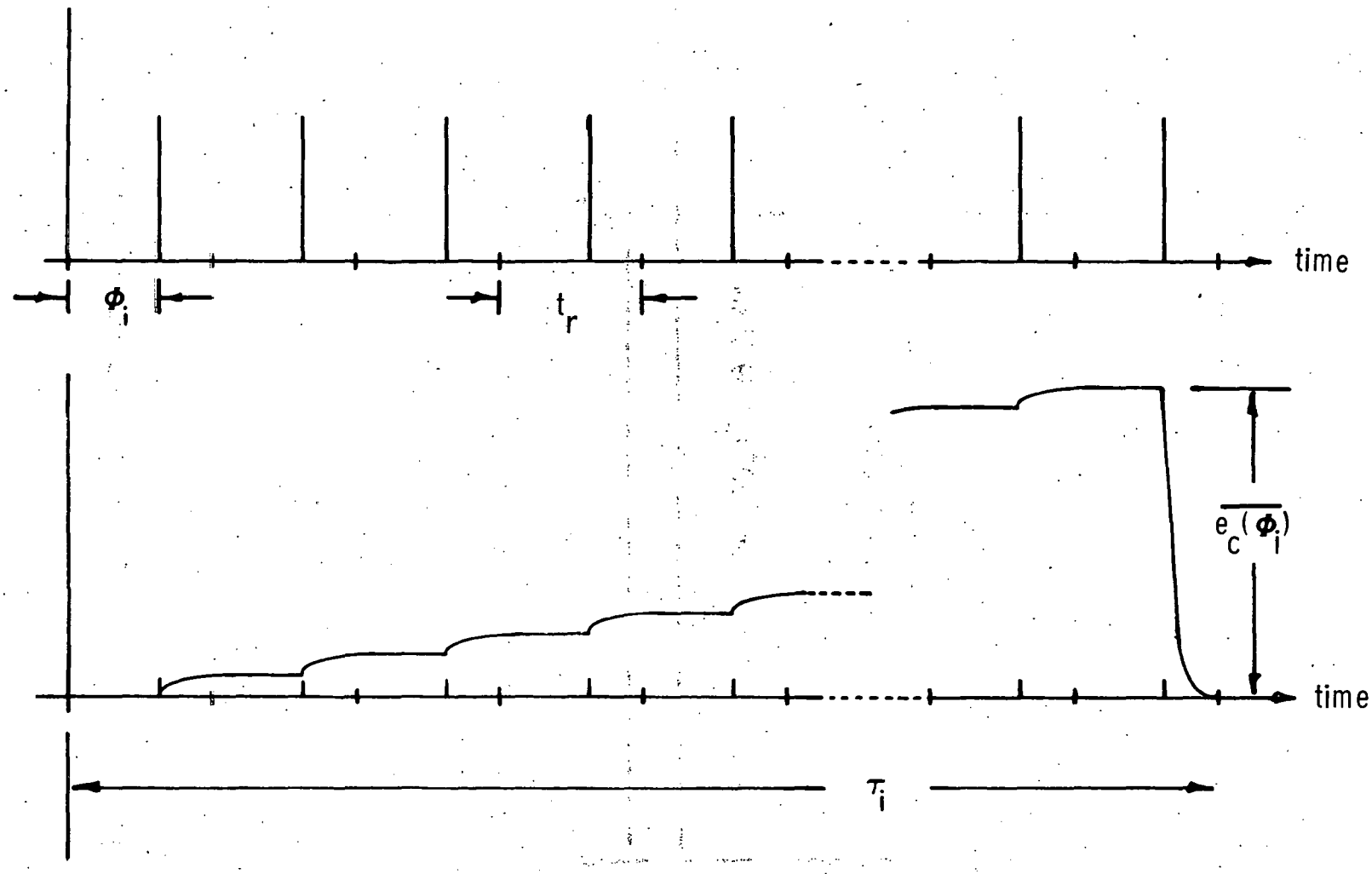

$\tau_i = 100\ t_r = 0.1524$ sec.

FIG. 17 DEVELOPMENT OF FINAL AVERAGED HETERODYNE SIGNAL

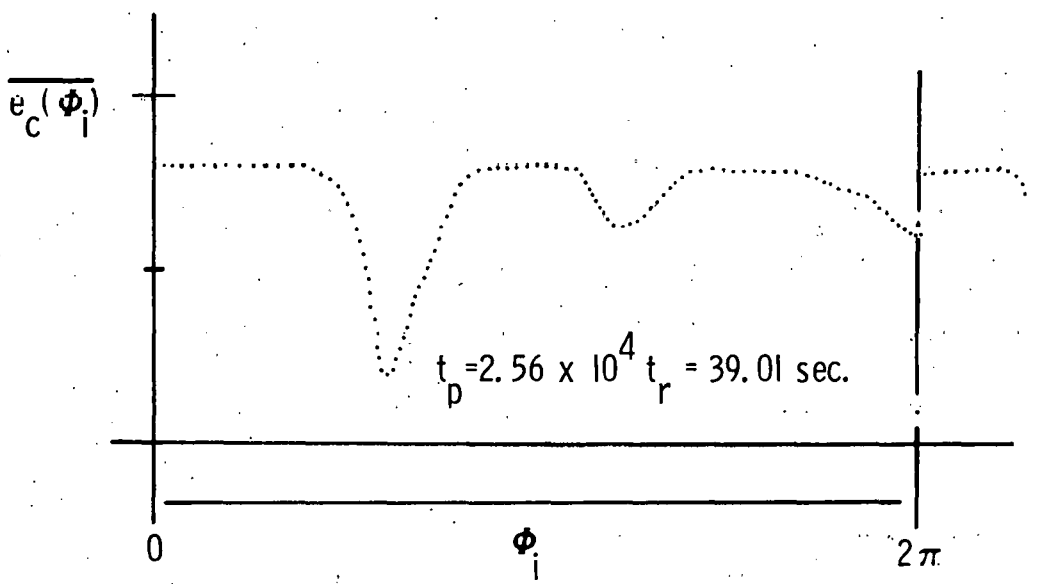

FIG. 18 DISCRETE FORM OF HETERODYNE SPECTRUM

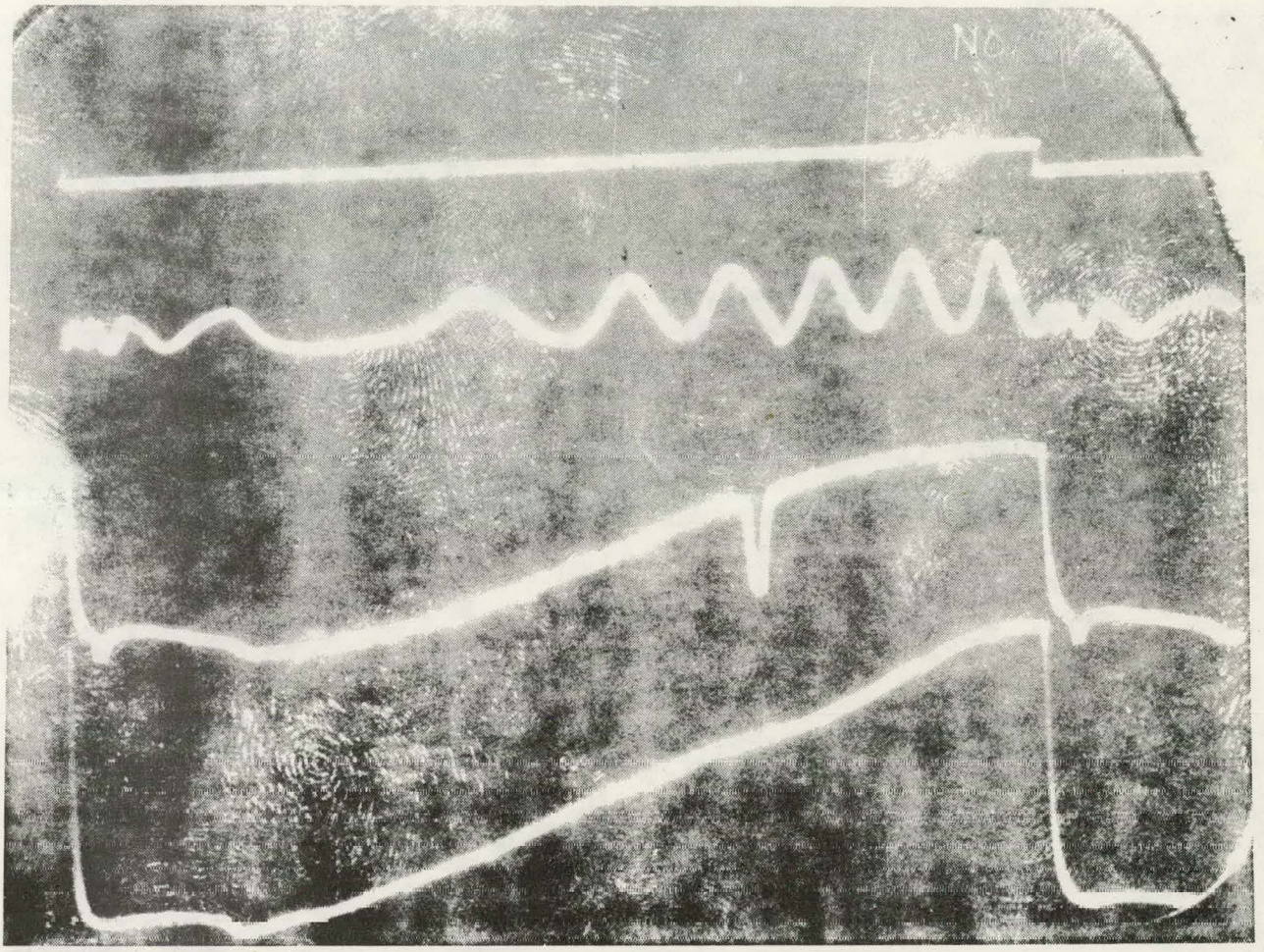

FIG. 19 SINGLE MODE OPERATION VERIFICATION TEST:

TRACE 1: CURRENT INJECTION RAMP

TRACE 2 : GERMANIUM ETALON IN PATH, SHOWING TYPICAL FREQUENCY MODULATION AND INHERENT TUNING NON-LINEARITY OF DIODE LASER SOURCE.

TRACE 3: NO ABSORPTION CELL IN PATH, SHOWING NO ABSORPTION LINE.

TRACE 4: NO CELL REMOVED, SHOWING INTRINSIC ABSORPTION

Note: The poor quality of this oscillograph was due in part to the fact it was taken about six hours before the balloon launch time.

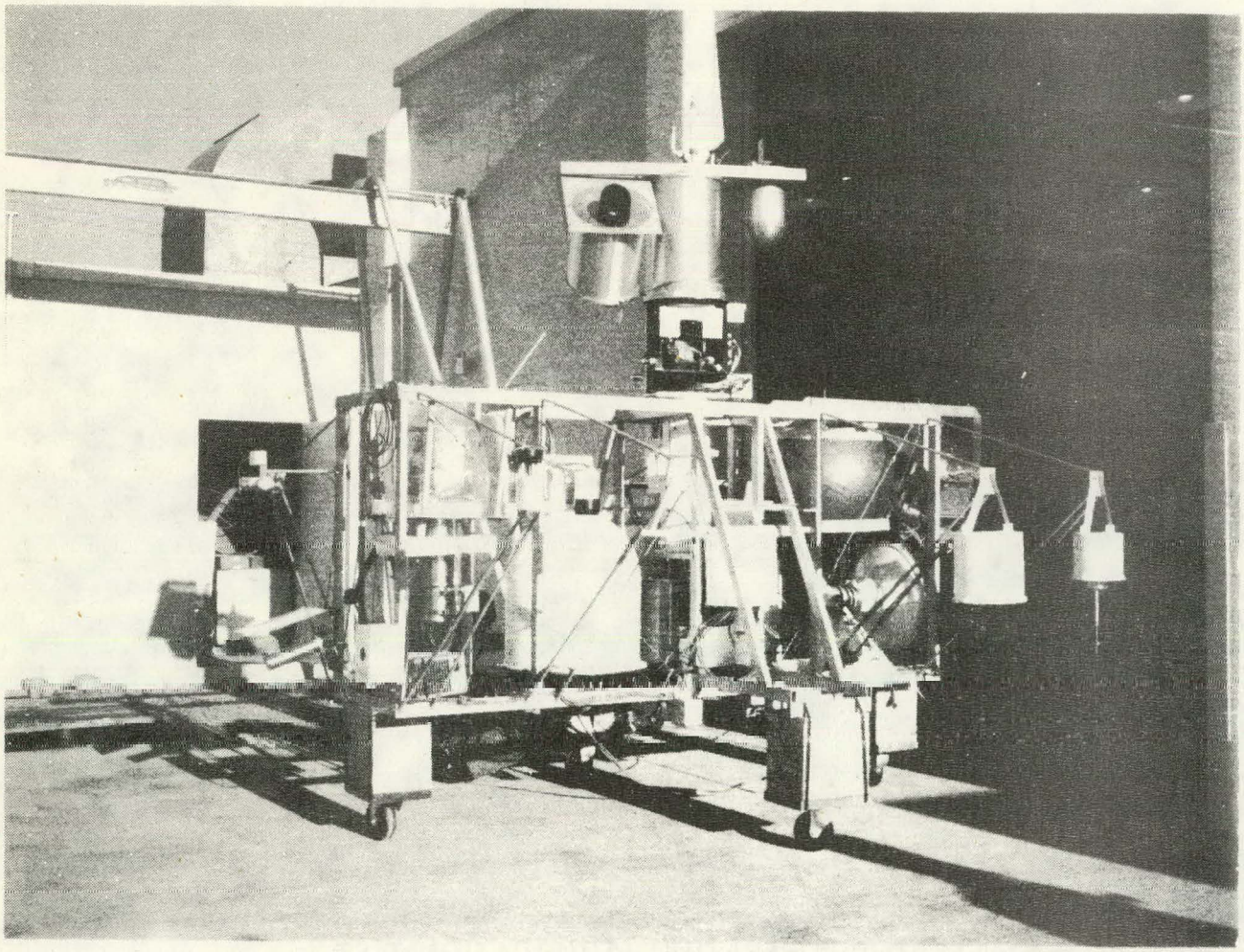

FIG. 20 PHOTOGRAPH SHOWING ENTIRE SCIENTIFIC INSTRUMENTATION PAYLOAD FOR 'STRATCOM VI' BALLOON FLIGHT. THE SOLAR HETERODYNE IS VISIBLE ON THE TOP, MOUNTED UPON THE SUN TRACKING MECHANISM. PAYLOAD WEIGHT 533 kgm.

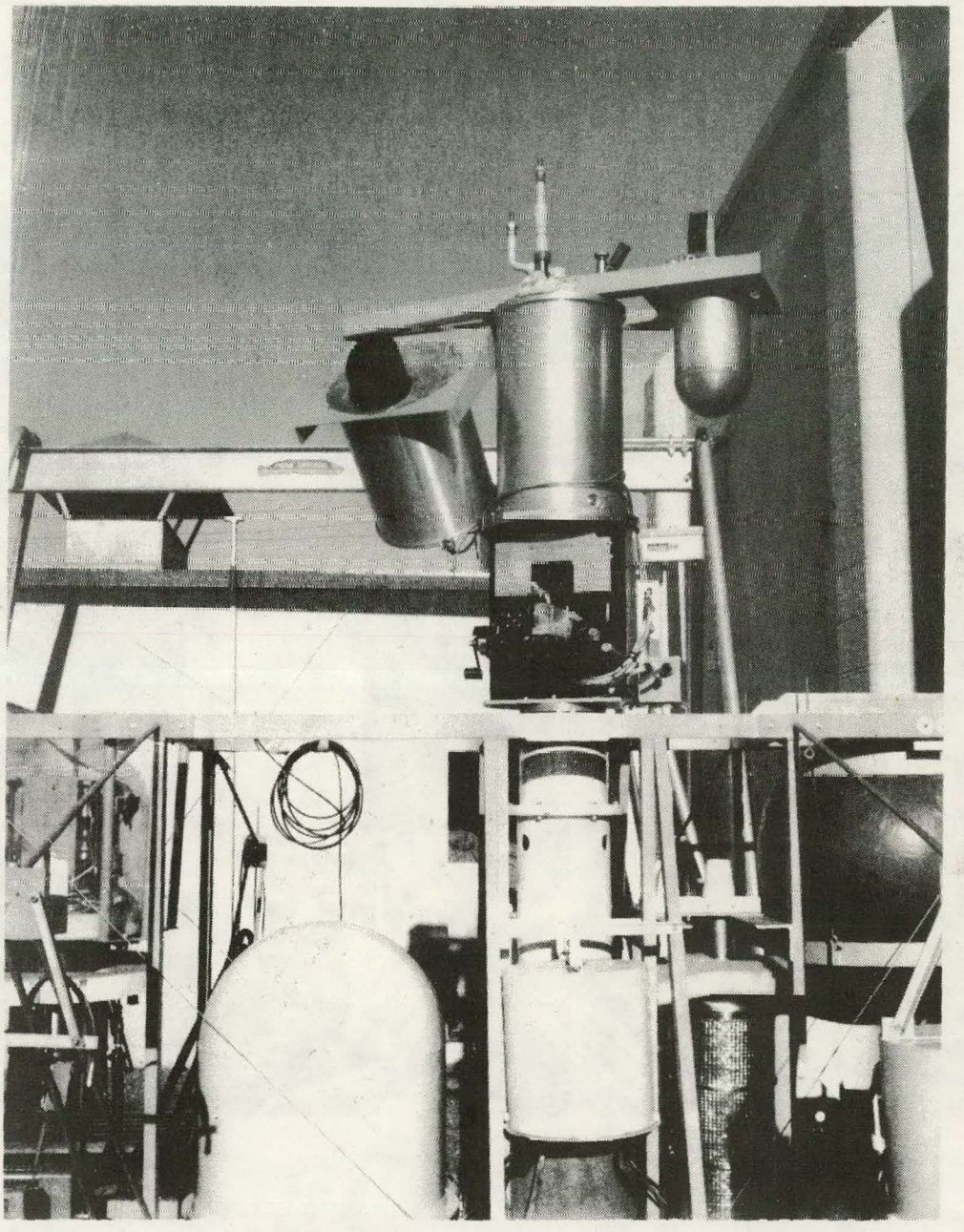

FIG. 21 PHOTOGRAPH OF SOLAR HETERODYNE RADIOMETER, SUN TRACKER AND ROTATIONAL PLATFORM INTERGRATED INTO THE 'STRATCOM VI' PAYLOAD.

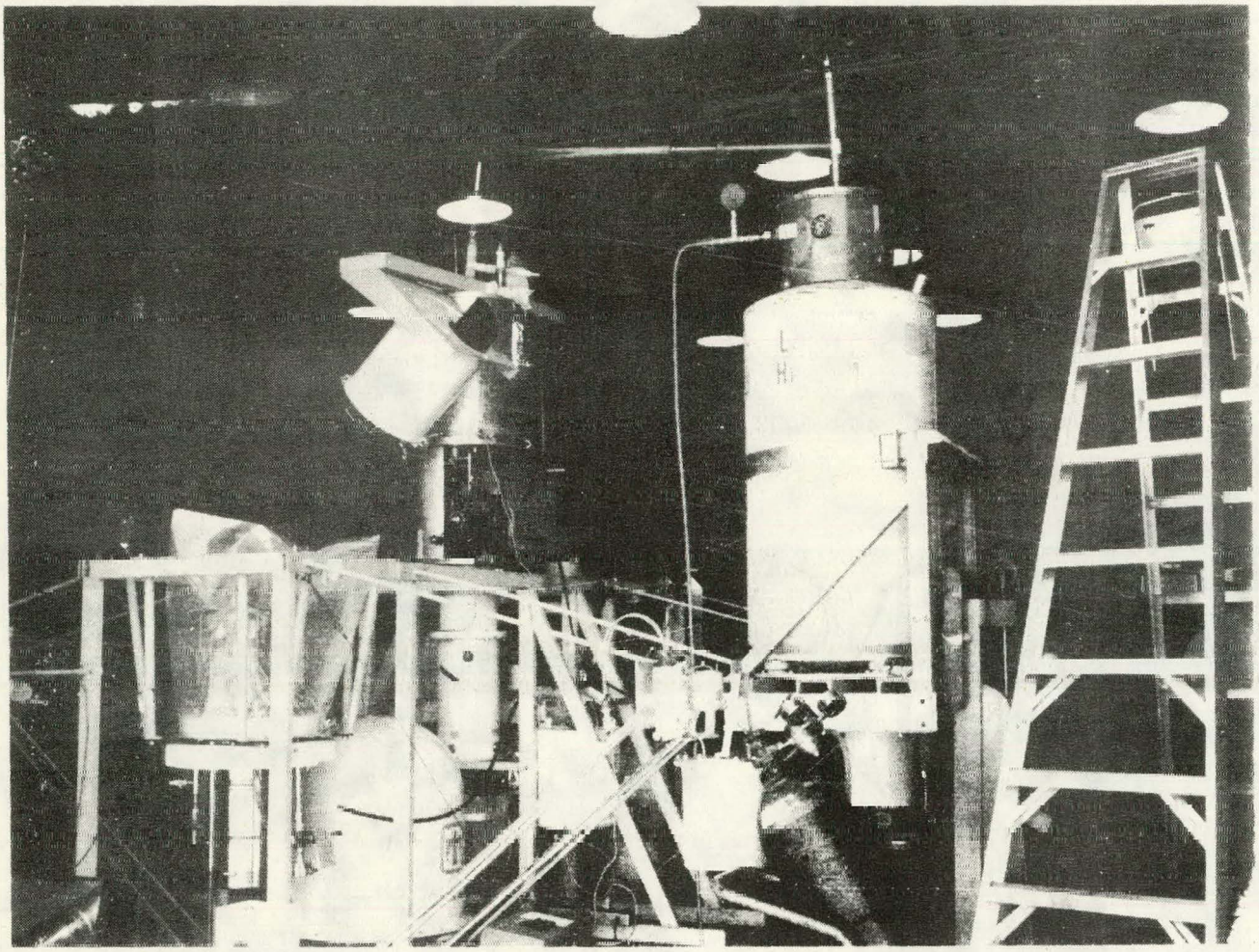

FIG. 22 LIQUID HELIUM TRANSFER OPERATION FOR SOLAR HETERODYNE RADIOMETER IN PLACE ON 'STRATCOM VI" PAYLOAD.

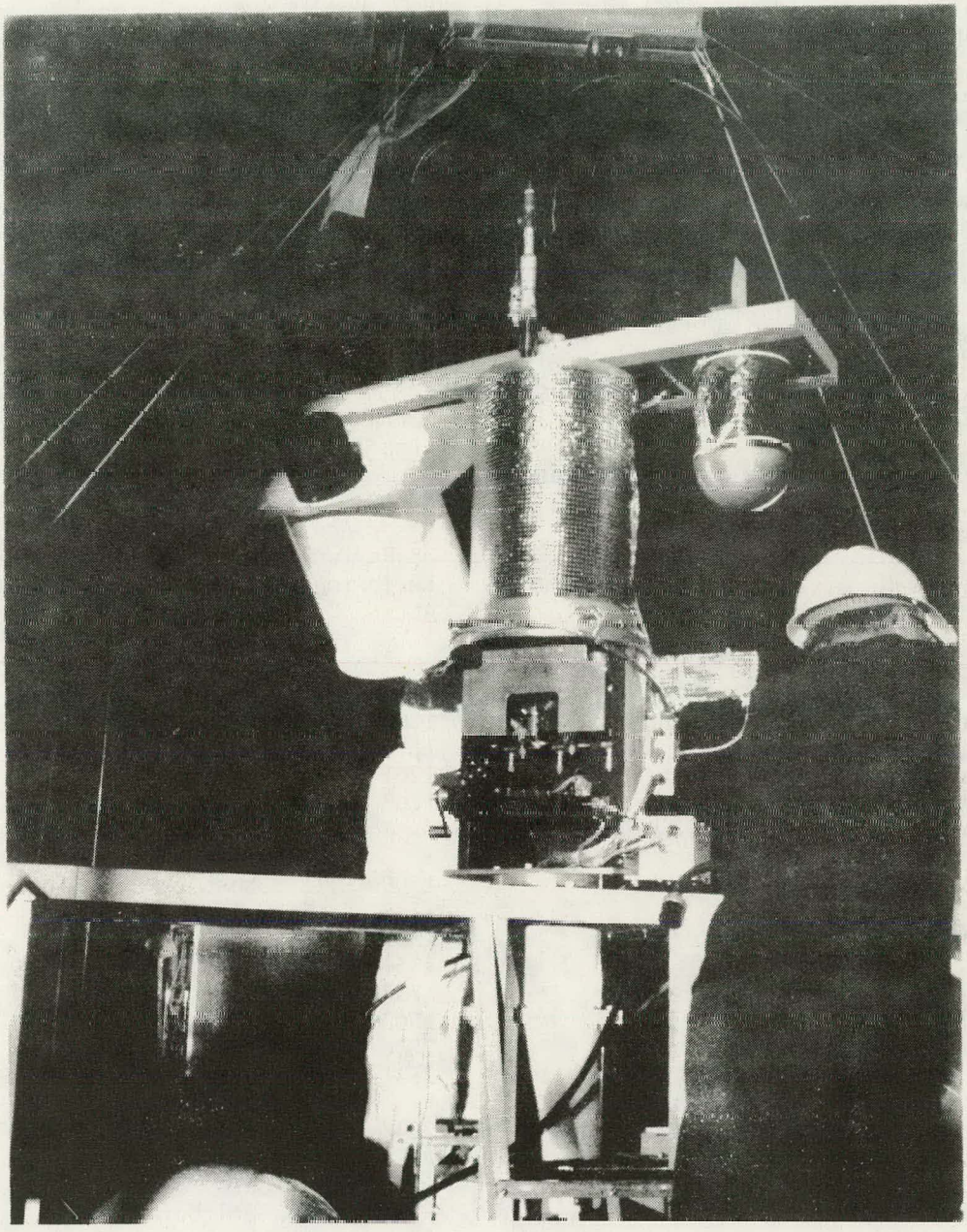

FIG. 23 SOLAR HETERODYNE RADIOMETER CONFIGURATION ONE HOUR BEFORE BALLOON LAUNCH TIME. NOTE: VENT LINES ARE ATTACHED AND CRYOGENIC SUPPORT SYSTEM IS PRESSURIZED.

DISTRIBUTION:

U.S. Air Force Weapons Laboratory (5)
Kirtland Air Force Base, N.M. 87117
Attn: Maj. Keith G. Gilbert/LRO-405
Capt. Terrence F. Deaton/ALO-400
Dr. David A. Depatie/ALO-405
Maj. Carl A. Forbrich, Jr./ALC-415
Dr. Leroy E. Wilson/ALC-415

U.S. Army Atmospheric Sciences Laboratory (2)
White Sands Missile Range, New Mexico 88002
Attn: Dr. Harold N. Ballard
Dr. Jaghir Randhawa

National Aeronautics & Space Administration (2)
Goddard Space Flight Center
Greenbelt, Maryland 20771
Attn: Dr. M. Mumma
Laboratory for Extraterrestrial Physics
Dr. J. Hillman
Infrared and Radio Astronomy Branch

NASA Langley Research Center (4)
Hampton, Virginia 23665
Attn: Dr. Frank Allario
Dr. R. K. Seals
Dr. Philip Brockman
Mr. R. V. Hess

Massachusetts Institute of Technology (5)
Lincoln Laboratory
Lexington, Massachusetts 02173
Attn: Dr. J. Melngailis
Solid State Assoc. Div. Head
Dr. A. Mooradian
Quantum Electronics Leader
Dr. A. G. Foyt
Applied Physics, Leader
Dr. D. L. Spears
Applied Physics
A. R. Calawa
Applied Physics

Massachusetts Institute of Technology (3)
Cambridge Massachusetts 02139
Attn: Prof. C. G. Fonstad
Electrical Engineering
Prof. Peter A. Wolfe
Physics
Prof. C. Forbes Dewey, Jr.
Mechanical Engineering

California Institute of Technology (2)
Jet Propulsion Laboratory
Pasadena, California 91103
Attn: Dr. R. T. Menzies
Dr. D. Hinkley

University of California (10)
Los Alamos Scientific Laboratory
P.O. Box 1664
Los Alamos, New Mexico 87544
Attn: K. Boyer, L-Division
C. P. Robinson, JUMPer
R. J. Jensen, JUMPer
E. Brock, L-DOT
Herbert Flicker, L-DOT
G. H. McCall, L-4
L. A. Booth, L-5
J. A. Sullivan, L-6
S. D. Rockwood, L-7
J. P. Aldridge, L-8

Bell Telephone Laboratories (2)
600 Mountain Avenue
Murray Hill, New Jersey 07974
Attn: Dr. C.K.N. Patel, 4E-436
R. J. Kerl, 1E-410

Laser Analytics, Inc. (2)
38 Hartwell Avenue
Lexington, Massachusetts 02173
Attn: Dr. J. F. Butler
Dr. K. Nill

1000 G. A. Fowler
1200 W. A. Gardner
1260 K. J. Touryan
1261 D. F. McVey
1262 H. C. Hardee
C. E. Hickox
C. L. Hackett (5)
1300 D. B. Shuster
1330 R. C. Maydew
1332 C. W. Peterson
1334 D. D. McBride
1757 R. D. Meyers
2000 E. D. Reed
2540 O. M. Stuetzer
2541 G. W. Gobeli
P. J. Hargis
2542 K. R. Hessel
M. J. Landry
5100 J. K. Galt
5150 J. E. Schirber
5200 E. H. Beckner
5210 J. B. Gerardo
5217 R. A. Hill
5400 A. W. Snyder
5423 J. E. Powell
D. A. McArthur
5700 J. H. Scott
5710 G. E. Brandvold
8110 A. N. Blackwell
8111 Alvin F. Baker
8115 Dan Hartley

Distribution:

8116 C. W. Robinson
8330 George W. Anderson
8333 Gunner L. Scholer
Robert J. Gallagher
8266 E. A. Aas (2)
3141 C. A. Pepmueller (Act'g.) (5)
3151 W. L. Garner (3)
For ERDA/TIC (Unlimited Release)
ERDA/TIC (25)
(R. P. Campbell, 3171-1)